

MODELING THE THERMAL-MECHANICAL EFFECTS OF PHASE CHANGE
MATERIALS IN LIGHTWEIGHT OPTICS

by

ALEX FRENCH

A thesis submitted to the faculty of
The University of North Carolina at Charlotte
in partial fulfillment of the requirements
for the degree of Master of Science in
Applied Energy and Electromechanical Engineering

Charlotte

2023

Approved by:

Dr. Wesley Williams

Dr. Beth Smith

Dr. Mesbah Uddin

©2023

ALEX FRENCH

ALL RIGHTS RESERVED

ABSTRACT

ALEX FRENCH. Modeling the Thermal-Mechanical Effects of Phase Change Materials in Lightweight Optics. (Under the direction of Dr. WESLEY WILLIAMS)

This thesis investigates the effects of adding a phase change material (PCM) such as paraffin wax to a lightweight optical component, specifically a mirror for directed energy applications. The goal of adding phase change material to the lightweight mirror is to reduce the temperature and deformation in the mirror under thermal loading, which would increase the system's optical performance. Lumped capacitance simulations performed in MATLAB Simscape showed that adding PCM to the optic reduced the maximum temperature by 58.6% (53.7°C). Subsequent thermal finite element analysis simulations performed in SolidWorks showed the expected relationship between areal density and the maximum temperature of the optic (i.e., lower areal density optics tend to have higher maximum temperatures and deformation), but also showed that the PCM's heat of fusion significantly contributed to lowering maximum temperatures achieved during multiple energy pulses. Thermal-mechanical finite element analysis additionally revealed that adding PCM to the optic reduced the mirror face deformation by 42.3% (2.0 μm) and the average temperature by 19.3% (7.9°C) after multiple energy pulses. The findings of this study could also be applied to other systems that require thermal management, such as renewable energy thermal storage and aerospace components. Ultimately, the results of this study suggest that embedding PCM into the backing of lightweight optics results in increased thermal capacity within the lightweight mirror allowing for increased dimensional stability which will increase the effectiveness by improving the quality of the beam on target due to the reduced distortion across the optic face.

DEDICATION

I would like to dedicate this thesis to my parents, Timothy, and Robin, for always believing in me and pushing me to accomplish things in my life that I would have never imagined myself. I am truly grateful for all the advice and support along the way to help me get to where I am today. Thank you for everything.

I would also like to dedicate this to the loving memory of my four grandparents that were unable to see this adventure unfold.

ACKNOWLEDGEMENTS

I would like to acknowledge the guidance and professional support Dr. Wesley Williams has offered throughout this thesis and my entire graduate school career. The completion of this thesis would not have been possible without Dr. Williams's volunteered time and resources.

I would also like to acknowledge the valued input and guidance Dr. Mesbah Uddin, Dr. Beth Smith, and Jacob Daniel offered during this process; their expertise and critiques weighed heavily in the completion of this thesis.

Table of Contents

Table of Tables	viii
Table of Figures	ix
List of Abbreviations.....	xii
Chapter 1 Introduction	1
Chapter 2 Literature Review.....	3
2.1 Directed Energy	3
2.2 Lightweight Optics.....	5
2.3 Phase Change Materials	9
Chapter 3 Methodology.....	13
3.1 Materials Selection.....	13
3.1.1 Optic Material	13
Chapter 3.1.2 Phase Change Material.....	14
3.2 Simulations	16
3.2.1 Lumped Capacitance Simulation	16
Energy Pulse.....	18
Lightweight Optic	18
3.2.2 Thermal Finite Element Analysis	21
Lightweight Optic Design	24
3.2.3 Thermal-Mechanical Finite Element Analysis	26

Chapter 4 Results	29
4.1 Lumped Capacitance Simulations.....	29
4.2 Thermal Finite Element Analysis	32
4.3 Thermal-Mechanical FEA	34
Variation A.....	37
Variation B	40
Variation C	43
Variation D.....	46
4.4 Highlights of Results.....	50
Chapter 5 Conclusion & Discussion	51
5.1 Lumped Capacitance Simulations.....	51
5.2 Thermal Finite Element Analysis	52
5.3 Thermal-Mechanical Finite Element Analysis	54
5.4 Future Work.....	57
References	59
Appendices	63
Appendix 1: 45 Isogrid Variations	63
Appendix 2: Custom PCM Block Code.....	64

Table of Tables

Table 2.2.1 Lightweight Optic Material Properties	7
Table 2.3.1 Phase Change Material Characteristics.....	11
Table 3.1.1 SiC Material Properties.....	14
Table 3.1.2 Paraffin Wax Material Properties	15
Table 4.3.1 Nine Isogrid Variation Simulation Results	34

Table of Figures

Figure 2.1.1 U.S. Army’s HELWS	4
Figure 2.1.2 U.S. Navy’s LWSD	4
Figure 2.1.3 How a Concentrated Solar-Thermal Power System Works.....	5
Figure 2.2.1 Additive Manufactured Lightweight Optics	6
Figure 2.2.2 Lightweight Optic Material Comparison.....	8
Figure 2.2.3 Isogrid Backing Structure	9
Figure 2.3.1 Energy Cycle for Solid to Liquid PCMs	10
Figure 2.3.2 Energy Storage Test Sample Configurations	12
Figure 3.2.1 Simscape Lumped Capacitance Model.....	17
Figure 3.2.2 3-D Representation of 1-D Model.....	17
Figure 3.2.3 Energy Pulse Subsystem.....	18
Figure 3.2.4 Lumped Capacitance Overview of Optic and PCM.....	19
Figure 3.2.5 Lightweight Optic Layer.....	20
Figure 3.2.6 Phase Change Material Layer	20
Figure 3.2.7 SolidWorks Quarter Symmetry Meshing	23
Figure 3.2.8 Isogrid Rib Thickness.....	25
Figure 3.2.9 Isogrid Rib Spacing	25
Figure 3.2.10 Exploded view of Isogrid with embedded PCM	27

Figure 4.1.1 Lumped Capacitance Simulation without PCM.....	30
Figure 4.1.2 Lumped Capacitance Simulation with PCM.....	31
Figure 4.1.3 Phase Change within Paraffin Wax at 308.2 degrees Kelvin	31
Figure 4.2.1 Isogrid Variation Areal Density	33
Figure 4.2.2 Isogrid Variation Maximum Temperature Result	34
Figure 4.3.1 Lightweight Optic Variation Chart.....	35
Figure 4.3.2 Variation A Backing with PCM.....	37
Figure 4.3.3 Variation A (Left) Without PCM (Right) With PCM	38
Figure 4.3.4 Variation A Maximum Temperature Comparison	39
Figure 4.3.5 Variation A Maximum Deformation Comparison	39
Figure 4.3.6 Variation B Backing with PCM	40
Figure 4.3.7 Variation B (Left) Without PCM (Right) With PCM	41
Figure 4.3.8 Variation B Maximum Temperature Comparison	42
Figure 4.3.9 Variation B Maximum Deformation Comparison	42
Figure 4.3.10 Variation C Backing with PCM	43
Figure 4.3.11 Variation C (Left) Without PCM (Right) With PCM	44
Figure 4.3.12 Variation C Maximum Temperature Comparison.....	45
Figure 4.3.13 Variation C Maximum Deformation Comparison.....	45
Figure 4.3.14 Variation D Backing with PCM.....	46
Figure 4.3.15 Variation D (Left) Without PCM (Right) With PCM	47

Figure 4.3.16 Variation D Maximum Temperature Comparison	47
Figure 4.3.17 Variation D Maximum Deformation Comparison	48
Figure 4.3.18 Variation A Energy Delivery Maximum Temperature Comparison.....	49
Figure 4.3.19 Variation A Energy Delivery Maximum Deformation Comparison.....	49
Figure 5.2.1 Isogrid 10-1 with PCM.....	53
Figure 5.2.2 Isogrid 14-1 with PCM.....	53
Figure 5.3.1 Thermal Displacement as a Function of Areal Density.....	54
Figure 5.3.2 Normalized Score Vs. Areal Density	55
Figure 5.3.3 Isogrid Variation Deformation Range Comparison	56

List of Abbreviations

1-D	One Dimensional
3-D	Three Dimensional
PCM	Phase Change Material
DE	Directed Energy
DEW	Directed Energy Weapon
FEA	Finite Element Analysis
SiC	Silicon Carbide
ROM	Reduced Order Model
CSP	Concentrated Solar Power
mg	Milligram
mm	Millimeters
PWM	Pulse Width Modulation
C	Celsius
J	Joules
kJ	Kilo-Joules
M	Meter
μm	Micrometer

W	Watts
ppm	Parts Per Million
MPa	Megapascal
GPa	Gigapascal
DOD	Department of Defense
HELWS	High Energy Laser Weapons System
LWSD	Laser Weapon System Demonstrator

Chapter 1 Introduction

Chapter 2 begins with a literature review of lightweight mirrors for directed energy applications. This overview examines the materials and design strategies used for realizing lightweight mirrors as well as the metrics which are used to assess mirror performance. Phase change materials (PCMs) are also reviewed in this chapter to provide an overview of the fundamental phenomenon of phase change, typical phase change material characteristics, and current trends in the development of high-performance PCMs.

Chapter 3 establishes the methodology for investigating the feasibility of using phase change materials to manage the thermal loads in lightweight directed energy mirrors. The three models of increasing fidelity used in this study were: lumped capacitance thermal modeling, thermal finite element analysis (FEA), and thermal-mechanical FEA. Lumped capacitance thermal modeling was performed in MATLAB SimScape, where the mirror geometry and phase change materials were modeled as thin discs with conductive heat transfer between them. Custom Simscape simulation blocks for the thermal mass of the phase change material were created to account for the heat of fusion that is absorbed at the transition temperature. These reduced order models (ROMs) provided insight into the impact of the PCMs on the overall thermal performance of the mirrors as well as the impact on the areal density of the mirror. Insights from the lumped capacitance models informed the design of 3D parametric models of a mirror with a lightweight Isogrid backing strategy that contained PCMs in the triangular backing pockets. Backing thickness and spacing were varied parametrically in search of optimal combinations for improved thermal performance (reduced maximum temperature) with modest increases in the areal density of the mirror. The best prospects from this parametric sweep are then subject to thermal mechanical modeling, where the thermal induced strains in the material were calculated

to assess the distortion of the optical surface, which is the ultimate driver of beam quality degradation.

Chapter 4 reports the lumped capacitance modeling, thermal FEA, and thermal-mechanical FEA results. As expected, the introduction of PCMs reduced the temperature rise of the mirror surface under directed energy exposure, with a modest increase in the areal density of the mirror. Additionally, the reduction in temperature minimizes the distortion due to quilting across the optical surface leading to improved beam quality and reliability of lightweight optics and the systems within which they are used.

Chapter 5 provides detailed conclusions gathered from the simulation results which provide insight into different backing designs and showcase the benefits of using PCMs to increase the thermal capacity in lightweight optics. Additionally, in this chapter, recommendations are made to build a framework for the potential future work to build upon the simulations conducted within this thesis.

Chapter 2 Literature Review

A literature review was conducted to investigate the existing technologies that relate to the topic of this thesis. Topics relating to directed energy, lightweight optics, and phase change materials were investigated.

2.1 Directed Energy

Directed energy (DE) can be defined in relation to energy such as weapons or concentrated solar. The DOD defines DE as: “*an umbrella term covering technologies that produce concentrated EM energy and atomic or subatomic particles. A DE weapon is a system using DE primarily as a means to incapacitate, damage, disable, or destroy enemy equipment, facilities, and/or personnel.*” [1]. In the development of directed energy weapons (DEW), a goal was to provide accurate low-cost “Per Shot” target engagement while simultaneously reducing potential collateral damage [1,2]. In the advancement of DEW, different challenges arise. The main challenges include the ability to effectively remove the immense amount of thermal energy generated by each pulse of the weapon [3]. Furthermore, issues regarding effective and accurate transfer of energy, such as beam distortion from optics under high thermomechanical loads, can cause quilting within the optics used [4]. Directed energy weapons have evolved as the technology has become more advanced. Some of the current models include the Army’s HELWS system equipped with a 15-kW laser seen in Figure 2.1.1, the Navy’s LWSD system that is equipped with a 150-kW laser seen in Figure 2.1.2, and Lockheed Martin’s layered laser defense system equipped with a 100-kW laser [5-7].



Figure 2.1.1 U.S. Army's HELWS ⁵

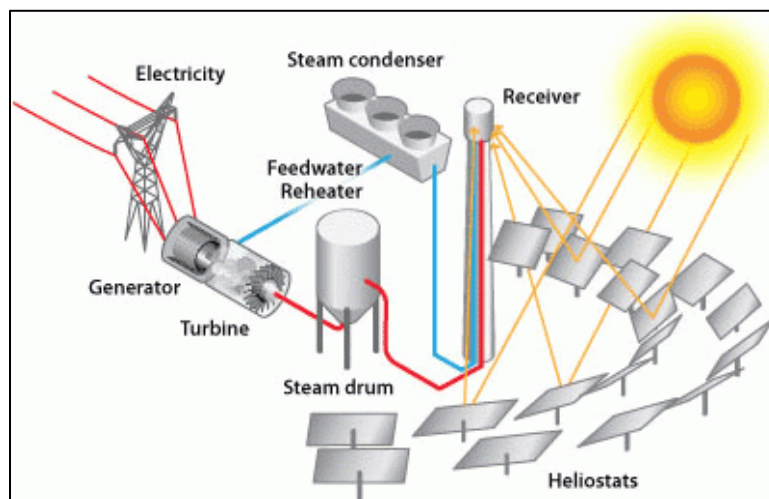


Figure 2.1.2 U.S. Navy's LWSD ⁷

Each potential application has different parameters requiring specific amounts of energy for effective function. The amount of energy that would be required is estimated to be around the range of $10,000 \frac{J}{cm^2}$, though this may vary depending on the material of the target [8].

In addition to DEWs, concentrated solar-thermal power (CSP) is under the umbrella of the term “Directed Energy”. The Department of Energy explains Concentrated solar-thermal power as “the use of mirrors to reflect and concentrate sunlight onto a receiver. The energy from the

concentrated sunlight heats a high-temperature fluid in the receiver” [9]. A graphical representation of how CSP systems work is shown in Figure 2.1.3.



*Figure 2.1.3 How a Concentrated Solar-Thermal Power System Works*¹⁰

Similar to the DEWs, CSP is reliant on the mirrors to reflect as much energy as possible to the receiver. Likewise, the potential deformation within the mirrors could cause inefficiencies reducing the overall performance of the system.

2.2 Lightweight Optics

Lightweight optics are designed with a balance between dimensional stability and the reduction of optic mass [11]. The increased stability and reduction of mass allow for configuration with lighter-weight attachments, ultimately reducing the overall weight of the system [12]. Current applications for these optics are various ground-based telescopes and satellite mounted space telescopes [11,13]. Another application where lightweight optics are used is within DEWs but is also known as adaptive optics. Although all the applications for lightweight optics use different sizes, they all incur similar issues while designing the lightweight optic. A method to develop optics with a reduced mass and increased stability is by

manufacturing the optics using additive manufacturing processes. These processes include direct metal laser sintering, electron beam melting, and binder jet [14]. A few optics can be seen within Figure 2.2.1 that have been additively manufactured.

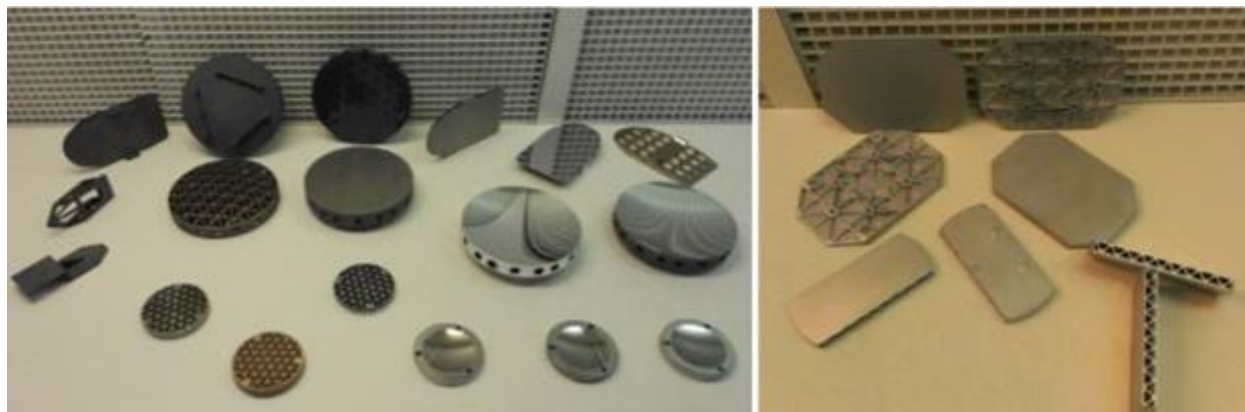


*Figure 2.2.1 Additive Manufactured Lightweight Optics*¹⁴

Previously to use these advanced manufacturing processes to develop lightweight optics, there were only a few materials to choose from. As the technology has improved over time, more materials have been incorporated into additive manufacturing processes. Choosing the right material to maintain dimensional stability and low mass is extremely important because during operation the properties of the material will change the response of the optic while under thermal loading. In space-bound applications, another element of complexity is added in considering the forces experienced by the optic during launch and while in transit to orbit [11]. In addition to the stress and strain from launch, the optics face an ever-evolving heat load during operation that can create noise within the optical system. Thus, raising the importance to reduce as much of the effects from temperature fluctuations as possible to allow for further development of space-bound telescopes [15]. The increased thermal loading of the optic over a certain time period would result in optic face distortion in the form of quilting. Quilting is a phenomenon

where the optic face is unable to disperse enough thermal energy in areas there is no backing present causing pockets of deformation and reducing the dimensional stability. To reduce the overall thermal loading of the optic while reducing the mass of the mirror, the material would have to have a high specific heat, high thermal conductivity, and a low coefficient of thermal expansion [13,16]. Some of the common materials that are used in lightweight optics that meet design criteria are aluminum (Al), beryllium (Be), silicon carbide (SiC), and zerodur as listed in Table 2.2.1 [12,17].

Table 2.2.1 Lightweight Optic Material Properties

Material	Density $\frac{g}{cm^3}$	Elastic Modulus (GPa)	Thermal Expansion $\frac{ppm}{K}$	Thermal Conductivity $\frac{W}{m * K}$
Aluminum	2.7	68	23.6	170
Beryllium	1.9	287	11.4	190
Silicon Carbide	2.55	218	2.0	170
Zerodur	2.5	92	0.0	1.6

Horvath and Davies use a simplified comparison of materials by characterizing the thermal stability of a variety of materials to choose the correct material [13]. Using the method that Horvath and Davies identified within their study to visualize the comparison of the material properties respective material properties in Table 2.2.1. The specific stiffness and steady-state thermal distortion can be calculated by using equations 2.1 and 2.2 respectively [13].

$$\text{EQN 2.1} \quad \textit{Specific Stiffness} = \frac{\textit{Elastic Modulus}}{\textit{Density}}$$

$$\text{EQN 2.2} \quad \textit{Steady State Deformation} = \frac{\textit{Thermal Conductivity}}{\textit{Thermal Expansion Coefficient}}$$

The results of those calculations can be represented by the specific stiffness of the material VS the steady state thermal deformation which can be seen in Figure 2.2.2.

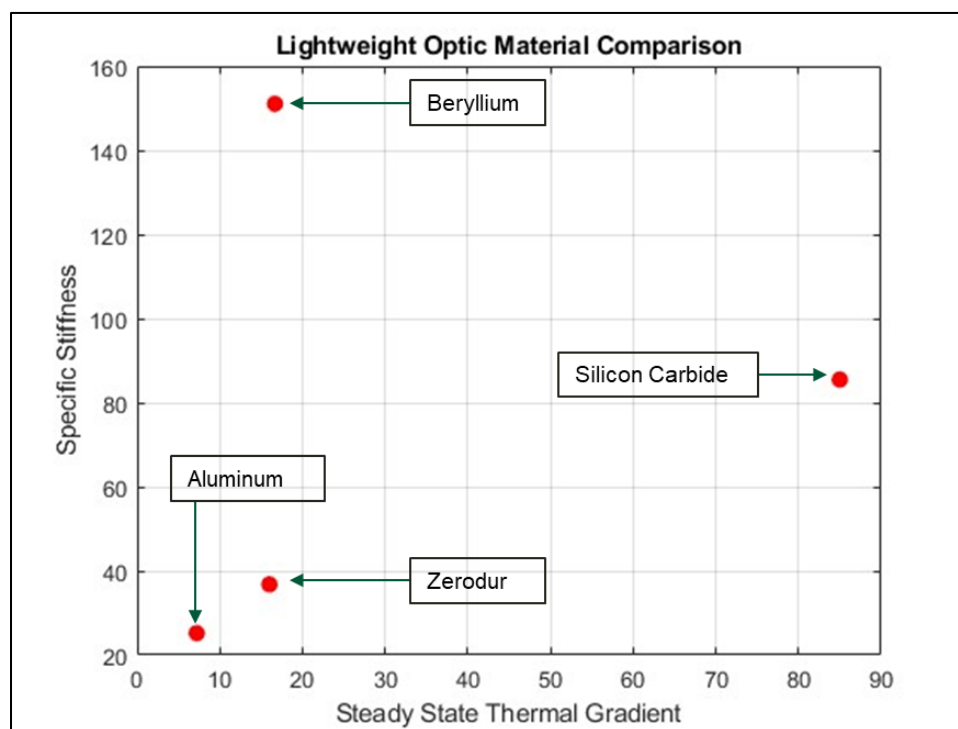


Figure 2.2.2 Lightweight Optic Material Comparison

As seen in Figure 2.2.2, SiC is the superior material due to the combination of its low density, increased specific stiffness, and better thermal conductivity which results in the best response to the thermal gradient [18]. Ultimately, SiC reflects the response that is desired in the optimization of a lightweight optic within this research.

In addition to the material selection, a lightweight optic backing design needed to be determined for use within this thesis. A common mirror backing design that was identified was

the Isogrid structure. This type of structure is used in other applications in addition to lightweight mirrors such as armor plates. The Isogrid structure is composed of a hollow, triangularly shaped pattern making a rib-like feature. Figure 2.2.3 shows an Isogrid backing for a lightweight mirror used in an investigation of different lightweight mirror configurations.[15]

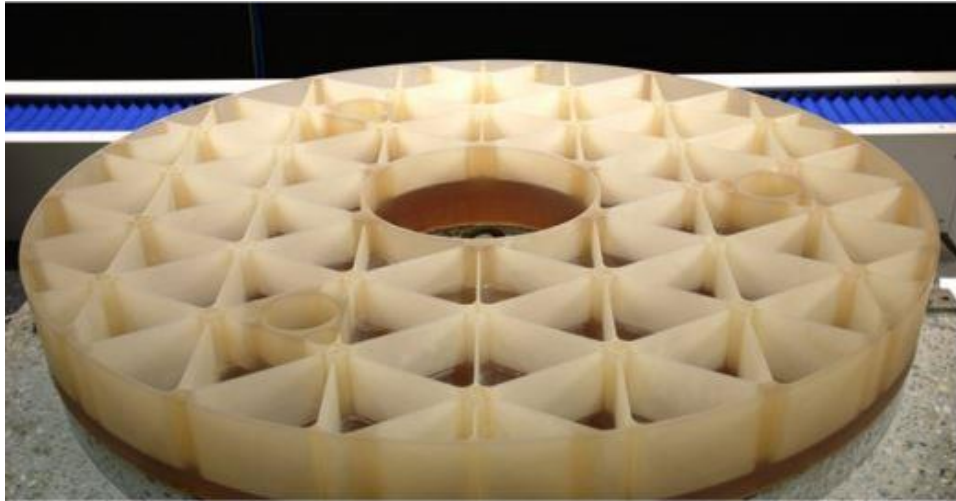


Figure 2.2.3 Isogrid Backing Structure ¹⁵

Due to the improved structural stiffness, the Isogrid-backing configuration is chosen coupled with SiC to be investigated within this thesis.

2.3 Phase Change Materials

Phase change materials are materials that undergo changes in their physical state when energy is added. Figure 2.3.1 shows how a solid-liquid PCM absorbs energy while in its solid state. The material will store the energy applied until a specific heat threshold is met which will change states into a liquid. Over time, as the PCM is cooled and energy is needed to be released, the material will begin to revert states back into a solid which was its original resting state [19,20].

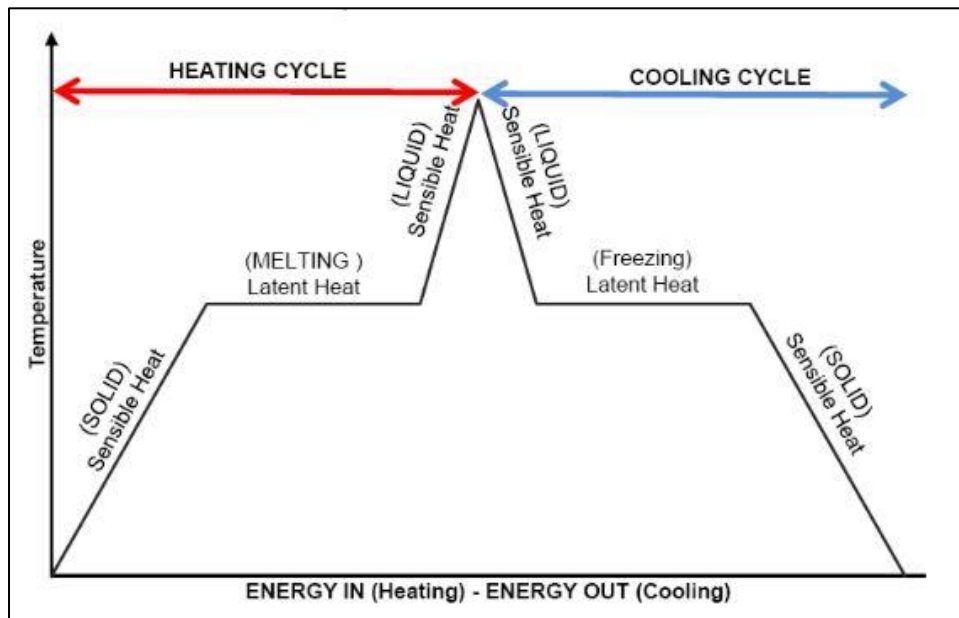


Figure 2.3.1 Energy Cycle for Solid to Liquid PCMs ²⁰

With many PCMs available to choose, such as paraffin wax, hydrated salts, and metallics, it is key to identify significant characteristics for each application. Corrosiveness, price, heat of fusion, weight, and melting temperature were considered in the modeling processes. Table 2.3.1 has the general characteristics for a few material types that point out the differences between them [21].

Table 2.3.1 Phase Change Material Characteristics

Property of PCM	Paraffin Wax	Hydrated Salts	Metallics
Heat of Fusion	High	High	Med.
Thermal Conductivity	Very Low	High	Very High
Melt Temperature (°C)	-20 to 100+	0 to 100+	150 to 800+
Latent Heat (kJ/kg)	200 to 280	60 to 300	25 to 100
Corrosive	Non-Corrosive	Corrosive	Varies
Cost	\$\$	\$	\$\$ to \$\$\$
Thermal Cycling	Stable	Unstable over Repeated Cycles	Stable
Weight	Medium	Light	Heavy

Paraffin wax is commonly used in low-cost thermal storage applications due to its ability to have the specific heat manipulated to the desired parameters of the application. This is commonly achieved by introducing other materials into the paraffin wax composition. Its non-corrosive characteristic makes it a good candidate to be used with a range of materials. Lastly, the stability of paraffin wax enables the continuous use within the temperature ranges ensuring the dependability of the material during operation [21,22].

Phase change materials are used in many different applications such as being used within a variety of heat exchangers and electronics to help control the temperature during use [23]. Another type of application for PCMs is being used as latent thermal energy storage for a system including being used in concentrated solar power where the thermal energy heats molten salt and then can be rapidly cooled creating steam to produce electricity [24]. In recent studies, Righetti

et al. have performed two studies into paraffin wax being used as a latent thermal energy storage undergoing thermal cycling to investigate the different reactions when PCM is embedded into different-sized structures and heated through its phase change to identify the most efficient configuration for latent thermal energy storage. A drawing of the samples used in this study is shown in Figure 2.3.2 [18].

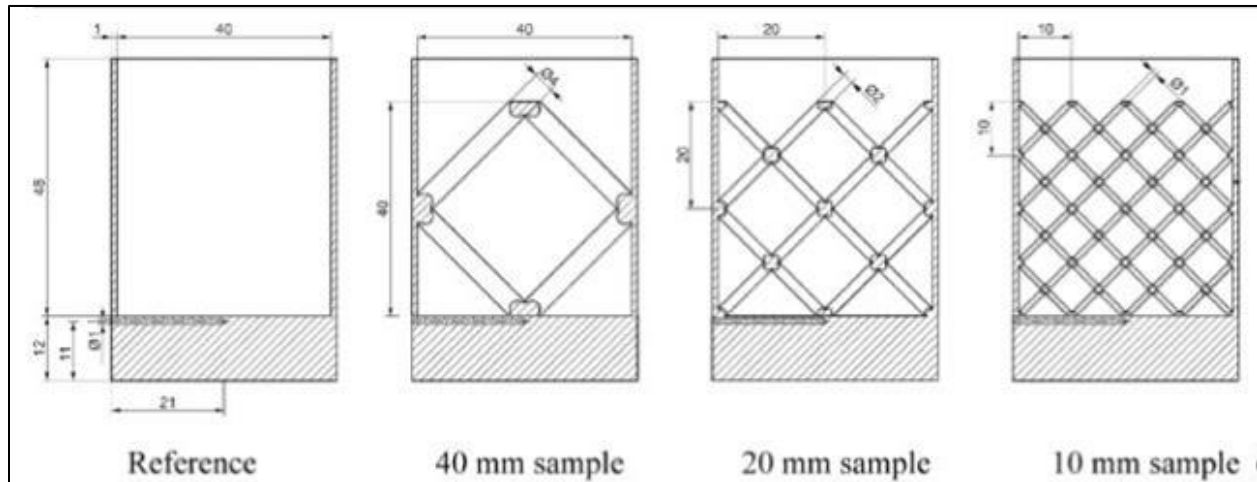


*Figure 2.3.2 Energy Storage Test Sample Configurations*¹⁸

Through testing, it was identified that when the PCM is dispersed into the smaller pockets, such as the 10 mm sample from Figure 2.3.2, it performs the best by producing a more consistent temperature dispersion across the sample. The 10 mm sample creates a more consistent temperature dispersion because of its increased surface area allowing for more PCM to be absorbed at any given time versus the larger samples such as the 40 mm sample that has a reduced surface area resulting in less PCM interaction and an uneven phase change [18].

Chapter 3 Methodology

The simulations of the directed energy PCM augmented mirrors are separated into two different types of methodologies: lumped capacitance simulations using MATLAB and Simscape, and 3-D finite element analysis simulations using SolidWorks. Having two different types of simulations enables initial exploration of the design space using the lumped capacitance model and further structural analysis of the mirror deformation from the applied thermal energy. In addition, using both types of simulations allow for generalized cross-validation that the simulations are performing as expected. Throughout categorized simulations, material properties and dimensions are identical to ensure comparability.

3.1 Materials Selection

3.1.1 Optic Material

Lightweight optics are designed for specific applications that may have distinct requirements, justifying a variety of different materials to be used to manufacture optics. As mentioned in Chapter 2.2, a few materials have taken the lead due to their improved performance. In a comparison of these materials, the material that has been chosen for this research is Silicon Carbide (SiC). This choice is made based on overall performance in lightweight applications and its prevalence in high-energy optics research. In Figure 2.2.2 it can be seen that Beryllium has a higher specific stiffness which might be desirable in some applications while SiC compromises by having a slightly smaller specific stiffness but an increase in thermal performance.

This compromise allows for the overall best material and potential performance for this optimization application. As a bonus, recent advancements in optic finishing allows for the SiC optic face to reduce its overall absorptivity to only 2% resulting in 98% of energy transfer

towards the target [25]. The material properties of SiC used in these simulations can be seen in Table 3.1.1.

Table 3.1.1 SiC Material Properties

Property	Value	Units
Elastic Modulus	218	GPa
Poisson's Ratio	0.14	N/A
Shear Modulus	218	GPa
Mass Density	2550	$\frac{kg}{m^3}$
Compressive Strength	3.9	GPa
Yield Strength	21	GPa
Thermal Expansion	2.00E-06	$\frac{1}{K}$
Thermal Conductivity	170	$\frac{W}{m*K}$
Specific Heat	750	$\frac{J}{kg*K}$

Chapter 3.1.2 Phase Change Material

Material advancements increase the effectiveness of phase change materials (PCM). As mentioned in Chapter 2.3 paraffin wax is an inexpensive material that is currently used in many different applications. Paraffin is an extremely versatile material that can be doped with other materials to increase the overall thermal capacity which ultimately changes the point of phase change from solid to liquid. In addition, the understanding that other PCMs potentially have

increased performance by using paraffin wax allows for the potential validation at lower performance bounds. Ensuring that if a PCM with an increased performance was implemented, it would potentially improve the results of these simulations. Therefore, paraffin wax has been chosen as the PCM for these simulations. The material properties of paraffin wax used in these simulations can be seen in Table 3.1.2.

Table 3.1.2 Paraffin Wax Material Properties

Property	Value	Units
Elastic Modulus	20	MPa
Poisson's Ratio	0.394	N/A
Shear Modulus	1.00E-06	MPa
Mass Density	834.36	$\frac{kg}{m^3}$
Compressive Strength	1.00E-06	MPa
Yield Strength	1	MPa
Thermal Expansion	6.00E-04	1/K
Thermal Conductivity	0.21	$\frac{W}{m \cdot K}$
Specific Heat	2890	$\frac{J}{kg \cdot K}$
Specific Heat @ PC	200000	$\frac{J}{kg \cdot K}$

To simplify and accurately simulate the phase change of the paraffin in both the lumped capacitance and FEA model, the specific heat remains the same until it reaches the temperature at which a phase change would occur. Then at the specified temperature, the specific heat is increased to the heat of fusion for the paraffin wax and then returns to the specific heat after the temperature increases past phase change temperature. The only difference from this process is that under physical testing as the temperature increases the specific heat would incrementally increase to the heat of fusion where it would change phases and then incrementally decrease to the specific heat of the original material.

3.2 Simulations

3.2.1 Lumped Capacitance Simulation

The lumped capacitance model within Simscape is a 1-dimensional model that is used to numerically investigate the hypothesis that adding PCM to lightweight optic structures will mitigate the transient thermal loading of the optic which theoretically would reduce the distortion of the mirror face and improve the performance of the optic. The Simscape model as mentioned previously contains the same material properties that the SolidWorks model uses to allow general validation in the Simscape model that the thermal simulations within Solidworks are performing as expected. The reason that it would not be an exact verification or validation of the model is that the lumped capacitance model does not account for the overall geometry of the optic backing, therefore, justifying the error in the two models. Another limitation that the current lumped capacitance model brings is only being able to simulate the temperature change those results from the laser pulses and not the physical deformation of the optic based on the thermal simulations. The Simscape model is broken into two sections, the energy pulse from the

laser and the lightweight optic. The full lumped capacitance model within SimScape can be seen in Figure 3.2.1.

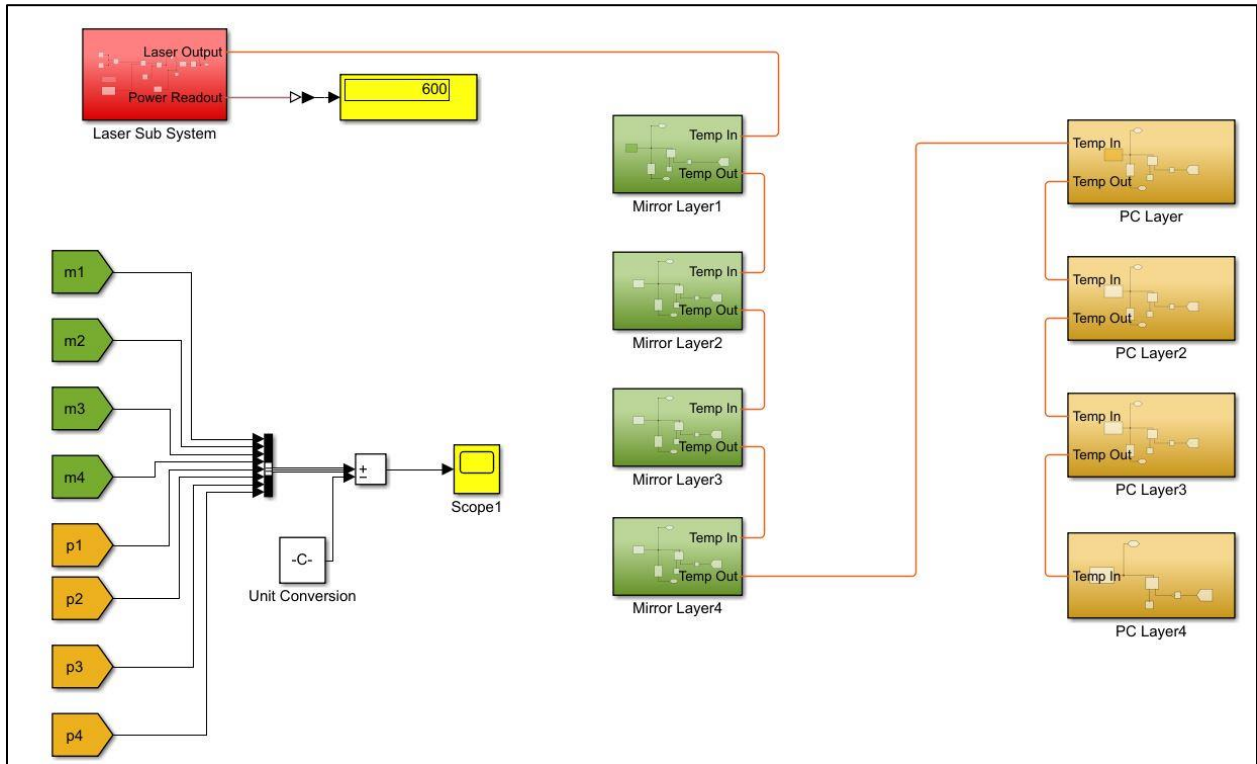


Figure 3.2.1 Simscape Lumped Capacitance Model

Figure 3.2.2 is a simplified representation of the 1D Simscape model to help better understand the flow of energy through the system.

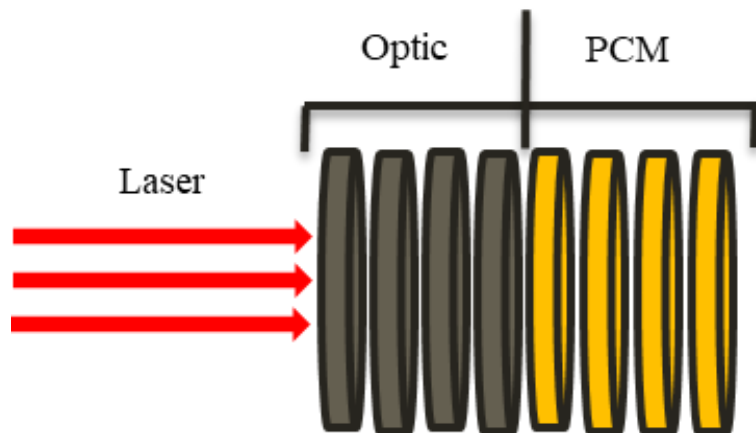


Figure 3.2.2 3-D Representation of 1-D Model

Energy Pulse

The energy pulse applied upon the lightweight optic material has been modeled to allow for both single pulses as well as multi-pulse simulations. The single pulse simulations are modeled with a step block added with a constant to enable power to be transferred to the mirror face. The multi-pulse simulations are modeled using a pulse width modulation (PWM) block. The PWM block allows for adjustability in the laser pulse's duty cycle, which can showcase different thermal responses within the optic. Both energy pulses are routed through a controlled heat source flow rate block and then through a conductive heat transfer block where it finally reaches the first layer of the optic. A high view of the energy pulse can be seen in Figure 3.2.3.

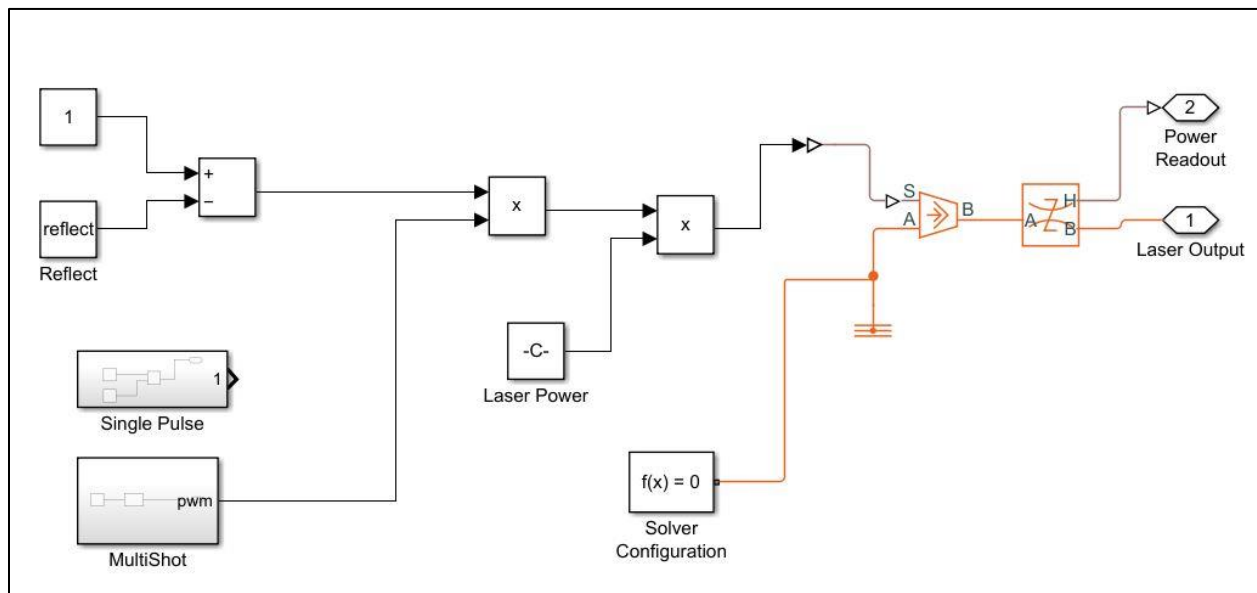


Figure 3.2.3 Energy Pulse Subsystem

Lightweight Optic

The lightweight optic portion of the model has also been designed for adjustability, enabling the lightweight mirror to be modeled in multiple ways without changing too many parameters. The easiest way is to model the mirror with a singular overall mass of SiC, this outputs a singular

temperature output for the whole optic. The second way (pursued in this research) to model the mirror is by breaking up the total mass of the SiC optic into multiple layers with conductive heat transfer between them. This is accomplished by modeling separate mass nodes with temperature probes to visualize the way the temperature increases through the layers of SiC, both models the singular layer and multi-layer models have the adjustability to include PCM in a singular layer or multilayer as well. In addition, the PCM can be removed to simulate the effects that are seen within only the SiC. The high-view layout of the optic and PCM can be seen in Figure 3.2.4.

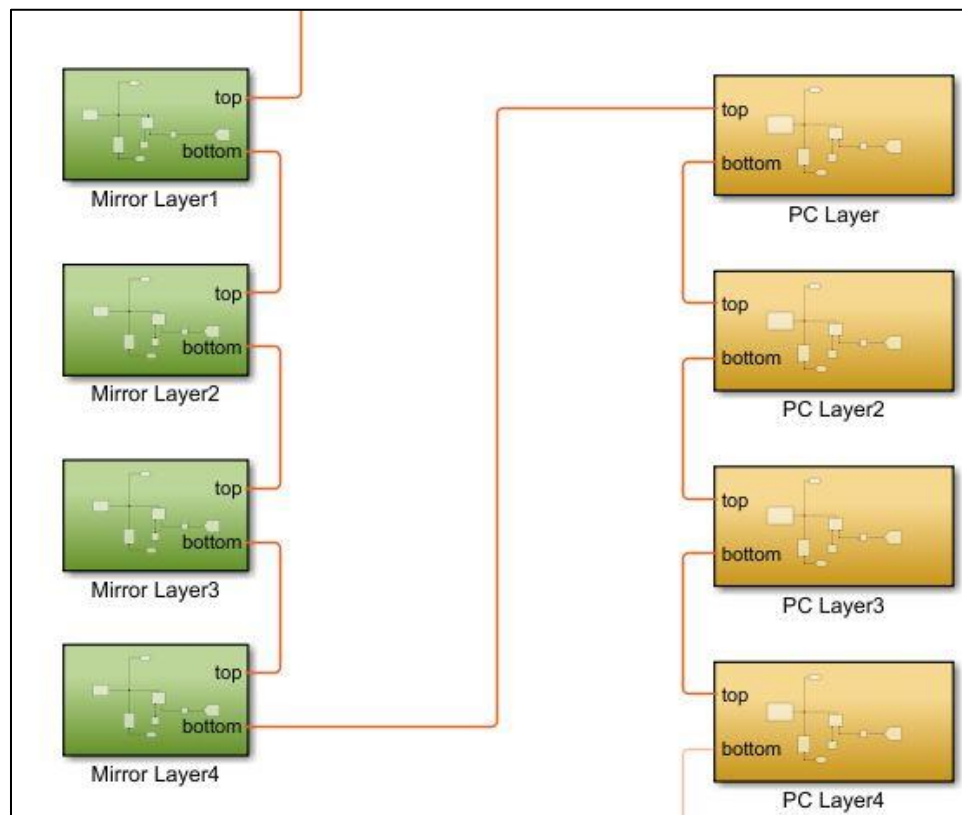


Figure 3.2.4 Lumped Capacitance Overview of Optic and PCM

Each material block holds a few components that are identical for all of the layers of each material. The blocks contained are a thermal mass to model the material, a temperature probe to identify the temperature at each layer, and then a conductive heat transfer component to the next

layer of material. The only difference between the optic layer and the PCM layers is that the PCM has a custom mass block to be able to vary the temperature in which the phase change occurs. The layer subsystems can be seen in Figure 3.2.5 and Figure 3.2.6 respectively.

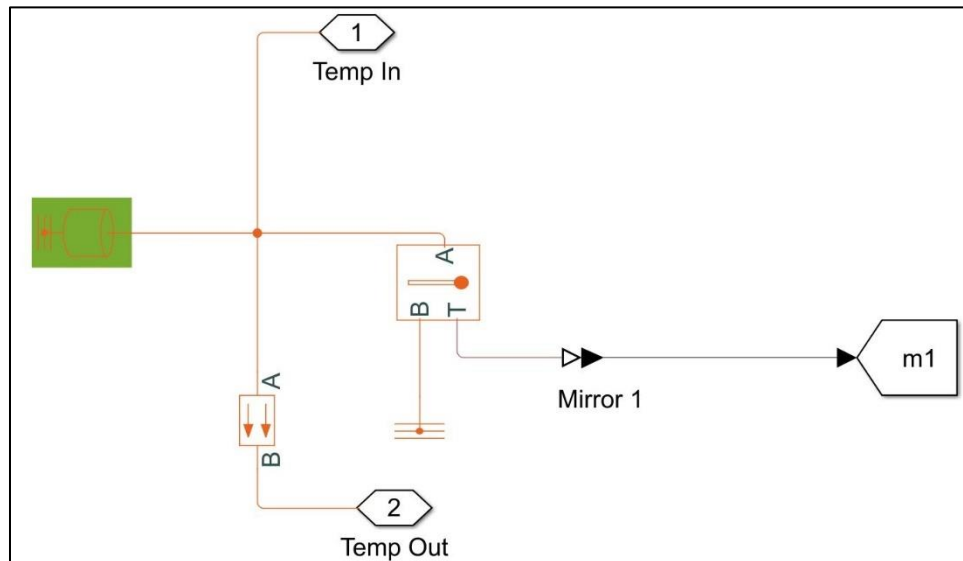


Figure 3.2.5 Lightweight Optic Layer

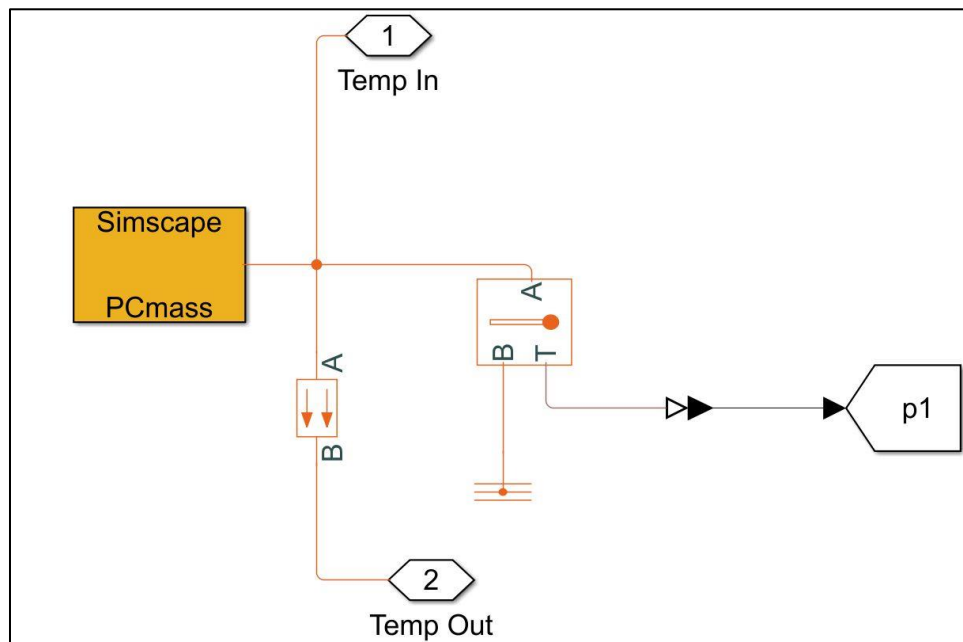


Figure 3.2.6 Phase Change Material Layer

3.2.2 Thermal Finite Element Analysis

The goal of creating a 3-D FEA simulation of the lightweight optic is to further expand on the lumped capacitance model in Simulink. The increased fidelity within the simulation allows for deeper analysis of the response when adding PCM into lightweight optics. In addition, the 3-D simulation provides details that are not shown in lumped capacitance modeling such as deformation caused by the increased thermal load. This deformation is caused by pockets of increased thermal loading in the face of the optic, commonly known as quilting. The presence of quilting ultimately results in a reduction in effectiveness due to the inability to effectively transfer the energy accurately to the target. Another benefit of performing thermo-mechanical simulations is provided by the visual comparison between optics with and without PCM embedded into the backing. SolidWorks was chosen as the software of choice for the wide variety of capabilities, such as being a modeling software with built-in FEA software with transient simulation capability. While also including the capabilities of taking results from a thermal simulation and use the results as initial conditions within a static study to be able to analyze the thermo-mechanical deformation that had occurred to the lightweight optic. Lastly, the ability to access through university licenses allowed for no expenses to be able simulations.

Simulation Parameters

Within SolidWorks two different types of simulations are being used, transient thermal and steady-state static simulations. As mentioned previously, throughout all the simulations, a quarter symmetry simulation technique was used to reduce the computational power required to perform simulations.

Thermal simulations were identical throughout the different sections of the optimization process. The initial condition of initial temperature was applied to all parts within the simulation

and set to 300 Kelvin or 26.9 degrees Celsius. To replicate the laser pulse, a heat power was applied to the face of the optic and was calculated by using Equation 3.2.1 & Equation 3.2.2 which resulted in 150 W.

$$\text{EQN 3.2.1} \quad \textit{Absorbed Energy Full Mirror} = (1 - \textit{Reflectivity}) * (\textit{Laser})$$

$$\text{EQN 3.2.2} \quad \textit{Absorbed Energy Quarter Mirror} = \left(\frac{1}{4}\right) * (\textit{Absorbed Full Mirror})$$

Then, within the heat power node, an adjustment to the time curve was made to replicate a 10% duty cycle where the heat power is applied for one second and then off for nine seconds. This combination of heat power with a 10% duty cycle is defined as a pulse or shot of the laser. Figure 3.2.7 illustrates the meshing parameters that were used for each simulation. Parameters that were used within a standard mesh configuration had a global size of 2.00 mm and a tolerance of 0.10 mm.

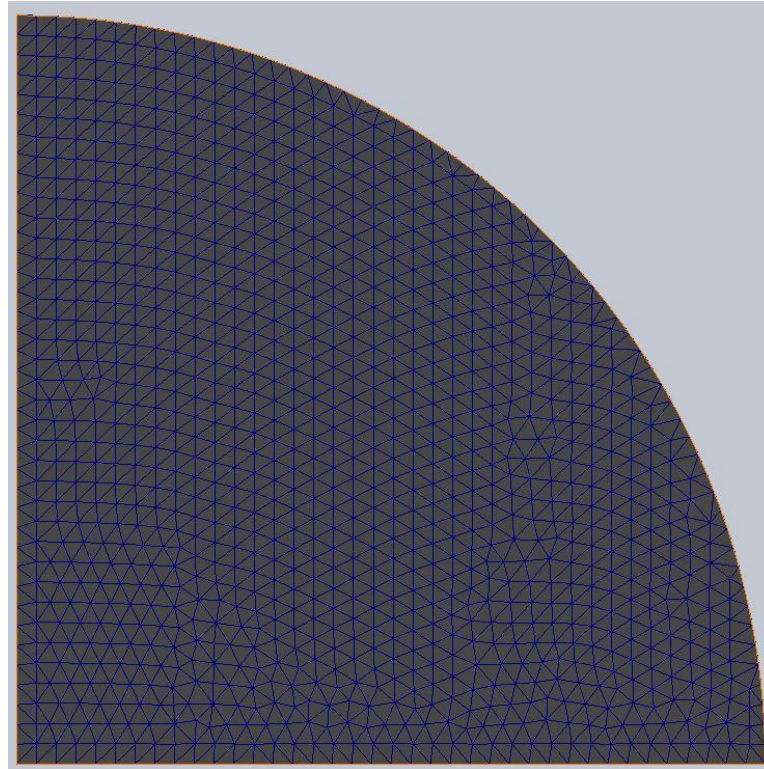


Figure 3.2.7 SolidWorks Quarter Symmetry Meshing

No convective or conductive cooling was added to the thermal simulations due to the wide variety of applications of lightweight optics. Not including cooling allows for a “worst case” in which the optic would have increased performance with additional cooling to the optic.

Parameters for the static simulation were also identical for all simulations in the optimization process. Initially, to account for symmetry, a symmetry fixture was applied within the simulation parameters, and a soft spring to stabilize the model was applied to show the true deformation of the optic alone. Additionally, a thermal load was applied to the model. During sections one and two of the optimization process, the thermal load was only after the first pulse of the laser but during the third section, the thermal loading was adjusted through the six static simulations to signify the deformation after each simulation. Lastly, the mesh for the static simulations was identical to that of the thermal simulations.

Lightweight Optic Design

The lightweight optic developed in this research was designed by taking a combination of characteristics that were mentioned throughout various research papers outlined within 2.2 that would allow for a parametric design study to be performed. A few assumptions were made during the design to constrain the design study of the optic. Firstly, the mirror is designed with a flat face. This assumption is made due to a large distance between the optic and the potential target resulting in a large focal length. The large focal length results in a large radius curvature of the mirror by using a flat-faced lightweight optic. In addition, to reduce the computational power required, the simulations will take advantage of the quarter symmetry of the optic. This enables accurate results while requiring less time and computational power for each simulation to complete. Lastly, the mounting points were negated to isolate the performance of the lightweight optics and the PCM. Mounting strategies would vary based on application, and in general, including mounting points for the optic will increase the overall stiffness of the optic which would increase its performance against thermal distortion.

Optimization of Lightweight Optic

Lightweight optics have a breadth of applications and therefore can be optimized toward numerous ends. To optimize this optic the constraints of what would not be changed as well as the variables to be changed needed to be outlined. The constraints would be that the optic face would not change in size from the chosen 150 mm optic diameter and all the variations of the optic would remain at the same thickness of 2.5 mm face as well as backing thickness of 2.5 mm as well. Thus, resulting in a 5 mm thick lightweight optic. The variables that would be changed in this optimization process would be the backing rib thickness outlined in Figure 3.2.8 as well as the backing rib spacing outlined in Figure 3.2.9.

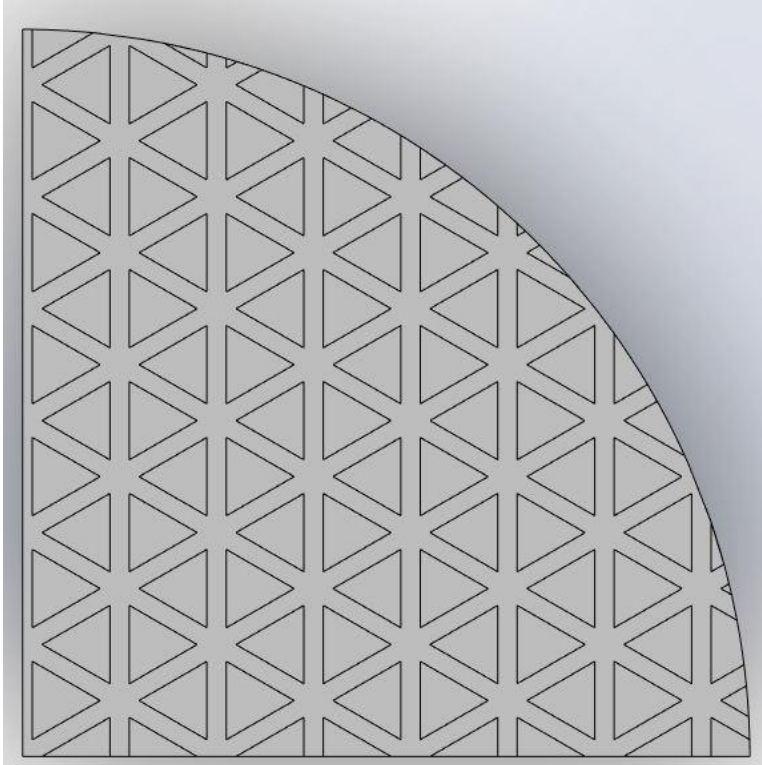


Figure 3.2.8 Isogrid Rib Thickness

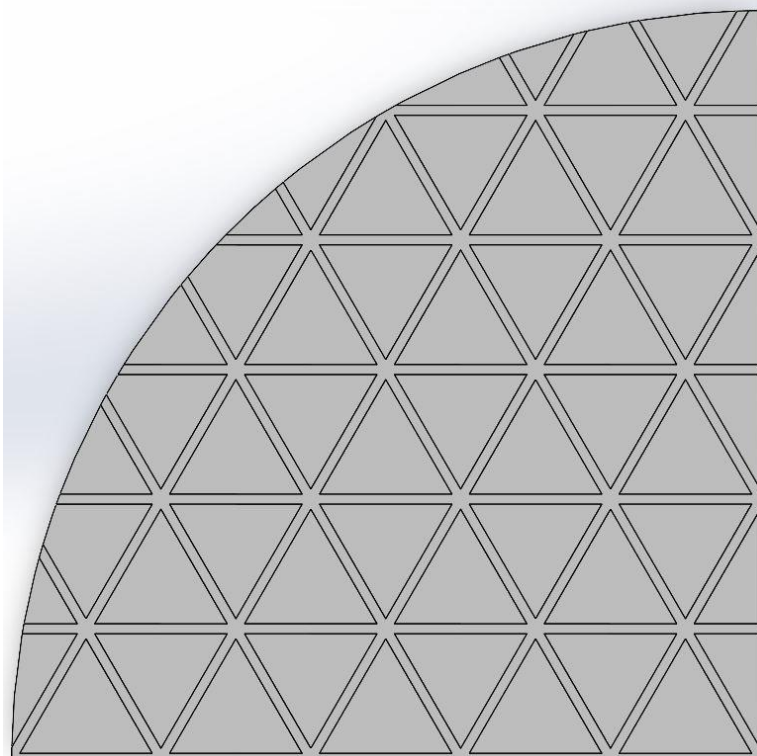


Figure 3.2.9 Isogrid Rib Spacing

To easily identify each optic, they each are named Isogrid Backing Spacing – Backing Thickness. For example, an optic with a backing spacing of 10 mm and a backing thickness of 1 mm would be called Isogrid 10-1.

The overall optimization process was divided into three different sections. The first section began with developing the initial criteria for backing design parameters to narrow down the total number of Isogrid designs. Initially, the lightweight optic was bounded between 10 mm and 14 mm for the backing rib spacing as well as bounded between 1 mm and 3 mm for the backing rib thickness. Both parameters would step 0.5 mm each parameter iteration until the limit was reached resulting in 45 total possible optic variations. Each of the 45 Isogrid variations without PCM would undergo a thermal simulation to find the maximum temperature and a static simulation with the thermal loads from the thermal simulation. The primary metrics to narrow the variations down are areal density, deformation from the static simulation, and max temperature from single shot transient simulation. To calculate the areal density, the mass of the mirror was calculated using SolidWorks and then plugging information into Equation 3.2.3 to get the result of each variation.

$$\text{EQN 3.2.3} \quad \text{Areal Density} = \left(\frac{\text{Mass of Optic}}{\text{Area of Optic Face}} \right)$$

3.2.3 Thermal-Mechanical Finite Element Analysis

The second section of the process was to narrow down the optic sizing, nine different Isogrid variations were chosen out of the original 45 Isogrid. These were chosen by taking four variations in each parameter's extreme. Additionally, five other Isogrid designs were chosen due to having abnormalities within their results such as a reduced temperature result after the single shot. With the identified designs, PCM was embedded into the backing design and the identical

single-shot transient simulation and static thermal deformation simulations were run. The exploded view of an Isogrid variation with PCM can be seen in Figure 3.2.10.

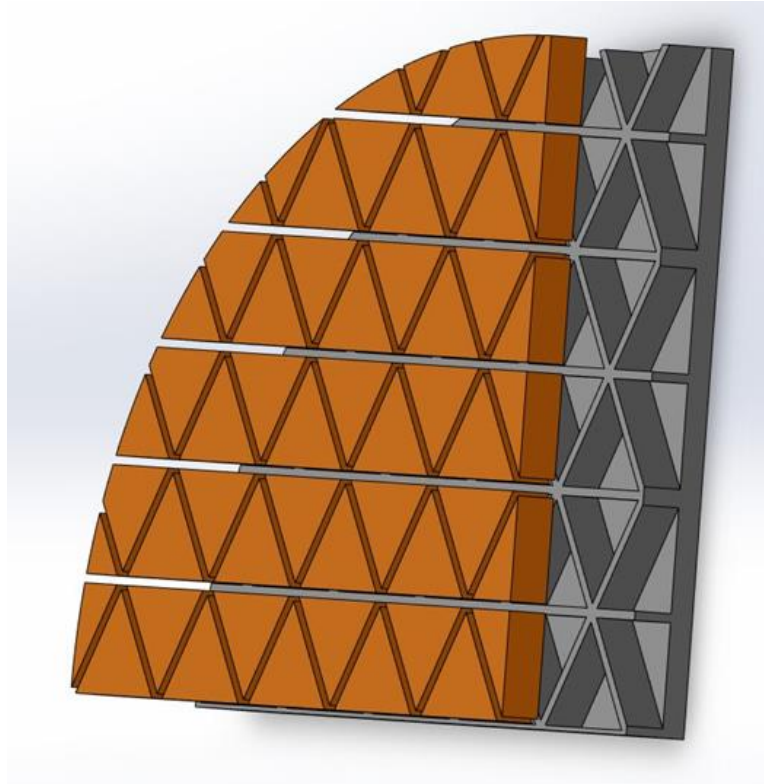


Figure 3.2.10 Exploded view of Isogrid with embedded PCM

As previously mentioned, lightweight optics are used in many different applications resulting in different parameters that are required for different applications. The parameters that might be optimized for the different applications might be but are not limited to reduced areal density, increased optic stiffness, and decreased temperature during operation. Therefore, within the third section of the simulation to showcase how the PCM will react in each of the various applications the highest performing Isogrid design in the previously mentioned parameters was chosen. Along with those three variations an additional optic was chosen by normalizing results using Equation 3.2.4 and selecting the highest-ranking design from the results.

EQN 3.2.4 *Normalized Optic = Aeral Density * Optic Face Displacement*

The four variations would undergo transient six-shot simulation with both PCM and without the PCM. Following the transient simulations, a static study after each of the shots and after 60 seconds was performed to compare the deformation over a period of time with and without PCM included.

The last simulation that would be performed is a comparison of pulsed power and constant power applied to the normalized optic with embedded phase change material. This simulation would use the same amount of power total, but the pulsed simulation would stay the same as previous simulations by being applied for one second and equating through the optic and PCM for the other nine seconds. The constant power would be the same power input but applied for six seconds straight. The energy applied to both optics would be 600 J for each pulse or 180 kJ while only 3.6 kJ total would be absorbed through the whole simulation. This simulation will show how the optic would perform under different conditions that might be seen during operation.

Chapter 4 Results

The simulation motivation, methodology, and processes have been outlined in the previous chapters. This chapter will showcase the results from the various simulations beginning with the lumped capacitance simulation modeled in Simulink. Then the second half of the chapter will showcase the 3-dimensional simulations modeled in SolidWorks.

4.1 Lumped Capacitance Simulations

As previously mentioned in Chapter 3, this simulation aims to build a model that will help effectively showcase the hypothesis that adding PCM to lightweight optic structures will mitigate the effects of the thermal loading of the optic. This in turn will theoretically improve the performance of the optic by reducing the overall deformation and the variation in deformation from quilting. The lumped capacitance model focuses on the effects thermally in a 1-dimensional aspect, negating the backing geometry of the optic. The result of running the outlined simulation for a period of 60 seconds without PCM can be seen in Figure 4.1.1, where the stepped temperature increase correlates with the periods of laser energy being applied to the optic. The energy added during these laser pulses is quickly distributed to the lower layers of the mirror via conduction, as there is no appreciable gradient between the four layers of the mirror material.

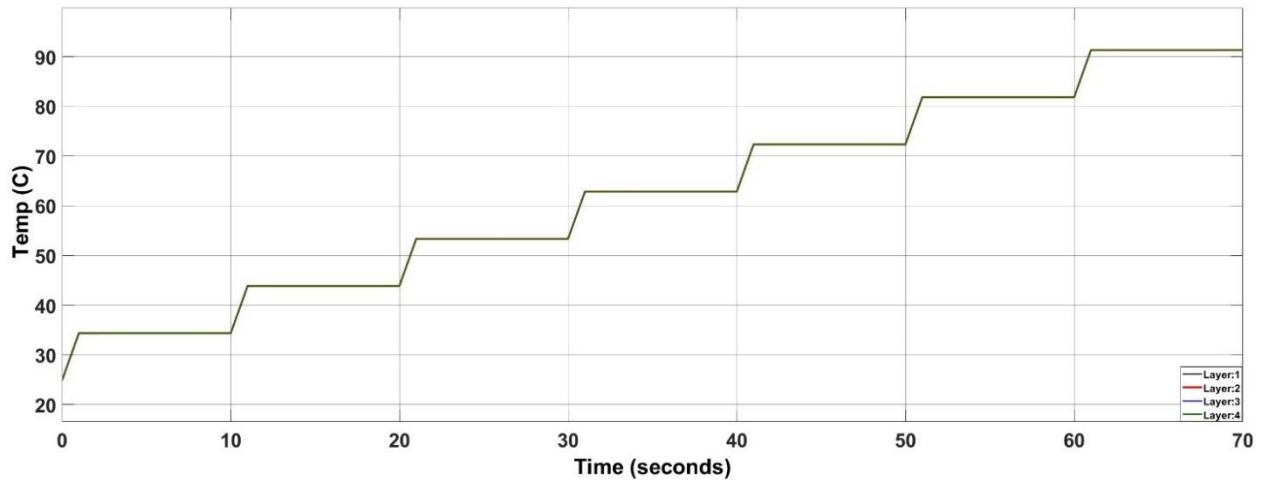


Figure 4.1.1 Lumped Capacitance Simulation without PCM

The same mirror surface is simulated again, but this time with PCM added as shown in Figure 4.1.2. As expected, following the one-second pulse of energy every ten seconds the temperature increases throughout the optic and PCM. The top layer of PCM reacts similarly to the optic material but the lower levels lag behind as the heat gets distributed through the system. Due to the large amount of energy that is required to change phases, the PCM will absorb most of the thermal energy that is injected into the system around that set temperature. Once enough energy has been absorbed to change phases the material optic will again begin increasing in temperature at a similar rate as before the phase change.

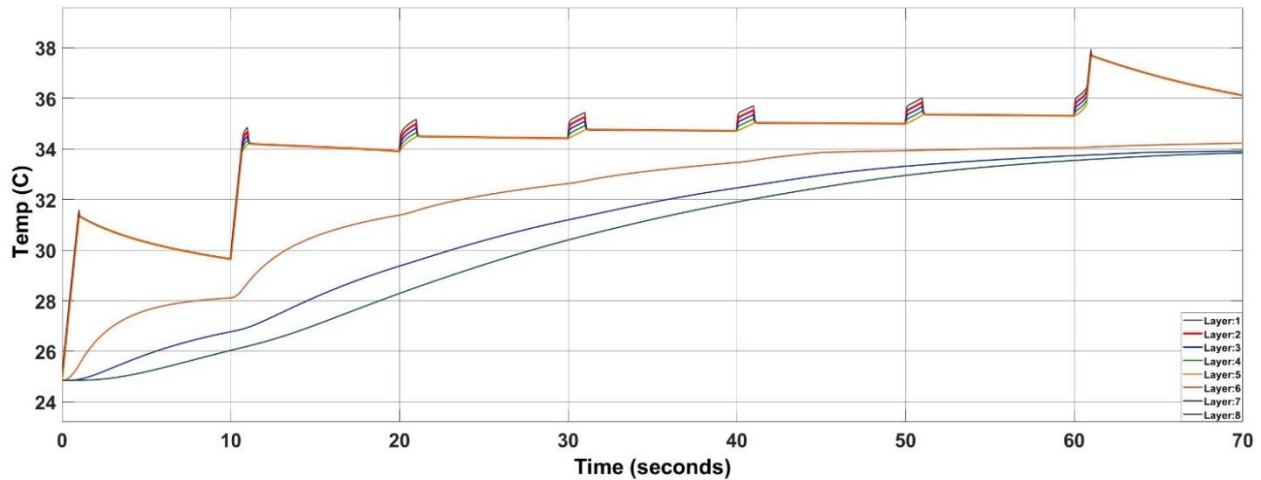


Figure 4.1.2 Lumped Capacitance Simulation with PCM

It is important to note that within these simulations, the PCM phase change is set to occur at 35 degrees Celsius or 308.2 degrees Kelvin. The lumped capacitance simulation can be broken down into three distinct sections which can be seen in Figure 4.1.3.

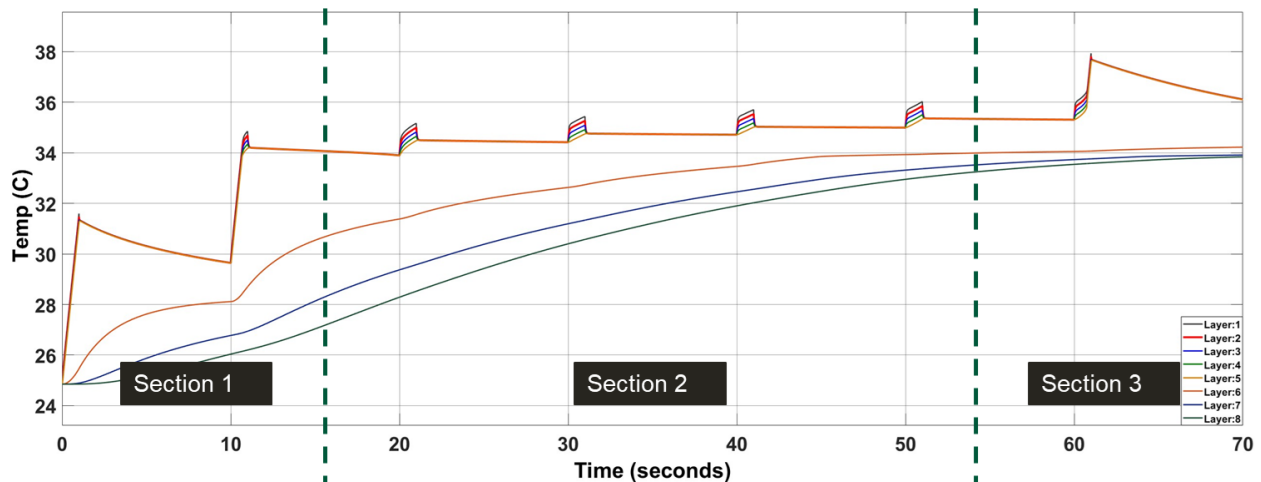


Figure 4.1.3 Phase Change within Paraffin Wax at 308.2 degrees Kelvin

Section 1 is where the first two shots of energy occur, raising the temperature to close to the phase change point of the PCM. Section 2 is the period of time where the PCM absorbs most of the energy that the optic is subjected to while completing its phase change. Section 3 is the

last section where the phase change is complete meaning the PCM is unable to absorb any more energy which results in the mirror material increasing again. The timing and results from these simulations are based upon the phase change set point as well as the materials chosen and the timing of the impact of PCM potentially could vary based on different materials. The overall addition of the PCM decreases the maximum temperature from 91.5 degrees C over 60 seconds to 37.9 degrees C. Resulting in a 58.6% improvement in maximum temperature.

4.2 Thermal Finite Element Analysis

The results of the lumped capacitance modeling showed the addition of PCM onto the backing of an optic reduced the temperature increase of the mirror surface. As a 1D model though it did not include any of the complexities of three-dimensional heat flow with respect to the backing structures of the lightweight mirror. The overall simulation methodology previously mentioned in Chapter 3 outlines the process of optimizing an Isogrid style optic backing along with the comparison simulations for different variations of Isogrid backings with and without PCM. Reiterating from Chapter 3, these SolidWorks simulations aim to build upon the lumped capacitance model by including the geometry of the optic backing. Expanding this simulation will provide increased accuracy to the effects that are seen when large amounts of thermal energy are applied. Initially, the optimization of the backing began without PCM and was parametrized by the spacing and thickness of the Isogrid ribs which created 45 different variations of backing designs. The important characteristics being monitored for each design are the areal density, max temperature after one pulse, and the max deformation after one pulse. After completing each simulation, the results were displayed on surface plots to showcase each

variation's respective characteristics which can be seen in Figure 4.2.1-4.2.2. All 45 different variations and statistics can be seen in a table in Appendix 1.

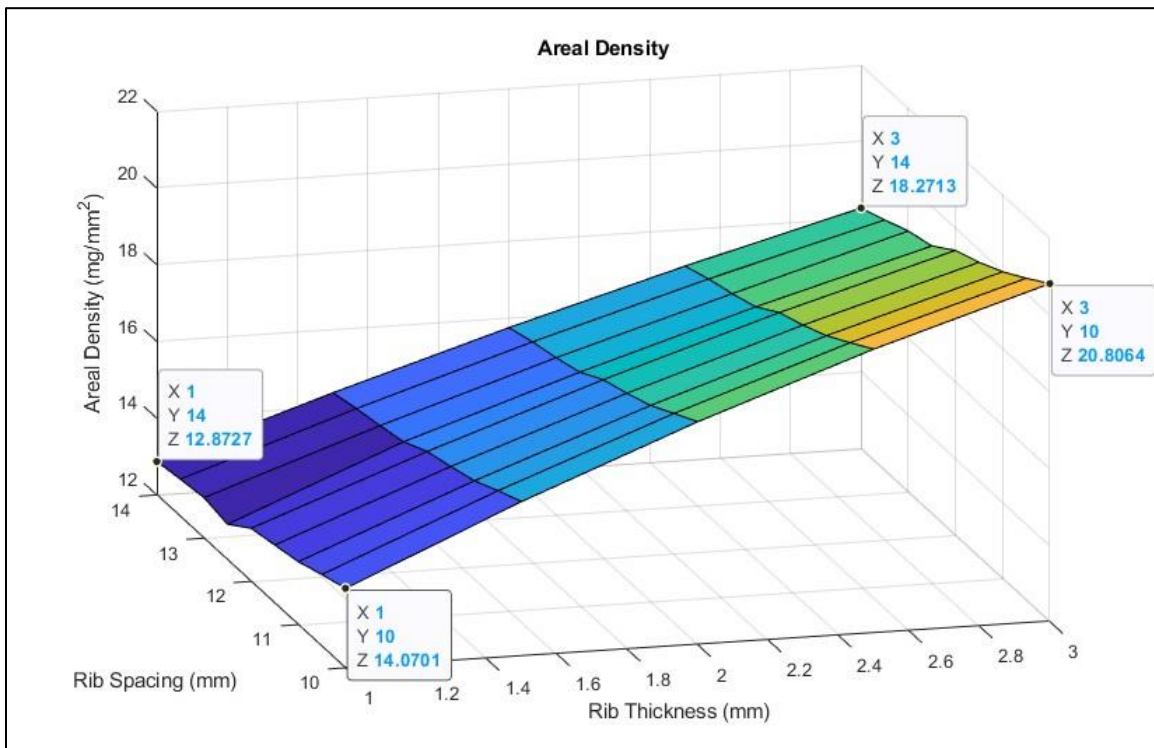


Figure 4.2.1 Isogrid Variation Areal Density

Figure 4.2.1 is a surface plot that plots the areal density against both rib spacing and rib thickness. Plotting the 45 variations in this format helps visualize how as the spacing or the thickness increases the areal density changes respectively. Whereas in Figure 4.2.2 areal density is replaced with the maximum temperature after a single pulse of energy. A relationship can be readily identified between the areal density and the maximum temperature, where a higher areal density results in a lower maximum temperature. Inversely, the lower areal density results in a higher maximum temperature. This matches the expectations for the models as higher areal densities correspond to larger thermal masses, and thus a greater resistance to changes in temperature.

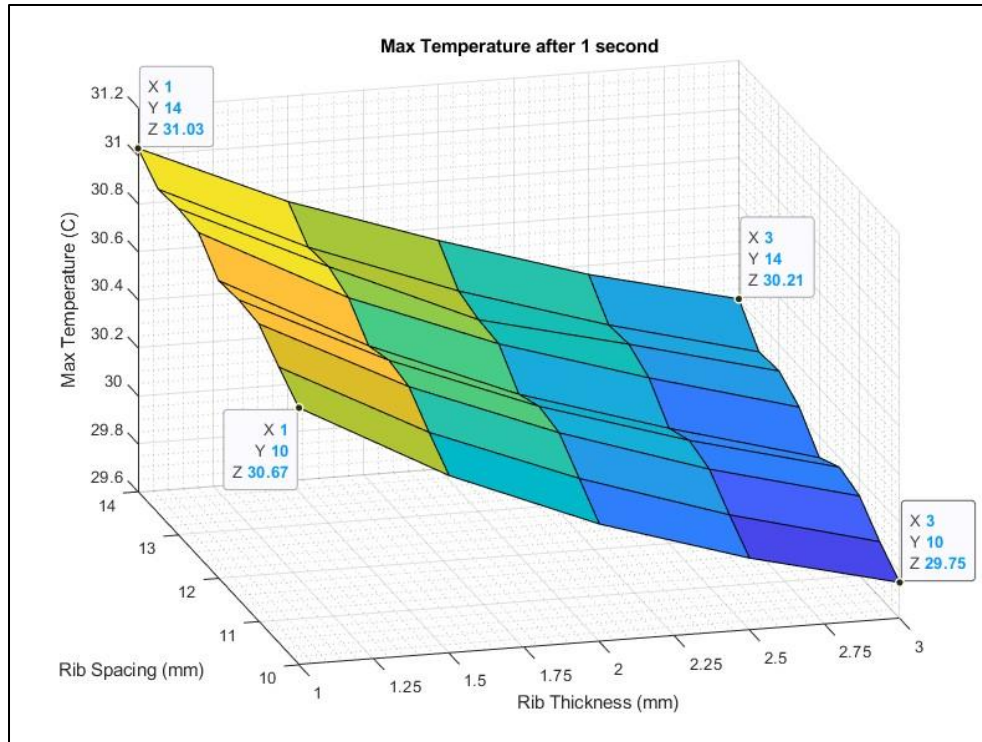


Figure 4.2.2 Isogrid Variation Maximum Temperature Result

Out of all the control (no PCM) variations, the one with the lowest temperature was Isogrid 10-3 with a maximum temperature of 29.8 degrees Celsius. To narrow the overall scope of the testing, the nine Isogrid variations that had the lowest temperatures after a single shot without PCM were selected to be tested again with PCM embedded into the backing geometry of the optic.

4.3 Thermal-Mechanical FEA

The nine variations that were chosen were subject to the same conditions as the prior testing to maintain the testing continuity. The results of the nine-variation single pulse transient studies are shown in Table 4.3.1

Table 4.3.1 Nine Isogrid Variation Simulation Results

	mm		mg/mm ²	C	M	Ge	Rank
	Mirror Spacing	Mirror Thickness	Areal Density	Max Temp 1 Second	Max Displacement		
1	10.0	1.0	17.0	32.1	1.32E-06	2.26	1.00
2	10.0	3.0	22.0	31.2	1.10E-06	2.43	5.00
3	11.5	1.5	17.9	31.7	1.34E-06	2.40	4.00
4	12.5	1.0	16.4	32.3	2.02E-06	3.31	8.00
5	12.5	1.5	17.6	32.1	1.89E-06	3.31	9.00
6	12.5	3.0	20.7	31.1	1.17E-06	2.43	6.00
7	13.5	1.5	17.4	31.9	1.38E-06	2.40	3.00
8	14.0	1.0	16.2	32.3	1.45E-06	2.34	2.00
9	14.0	3.0	20.2	31.3	1.22E-06	2.46	7.00

From these results, four different variations were identified to continue to the third phase of testing. Each variation was chosen due to having the best result in a specific characteristic. The characteristics were: the lowest areal density, lowest Maximum temperature, least amount of displacement, and an overall generalized score. The generalized score was calculated by multiplying the areal density by the maximum displacement. This score represents an optic that is balancing the overall mass and the amount of displacement making for an optic that is a compromise between the areal density and the displacement after one pulse on the optic. The chosen four Isogrid variations can be seen in Figure 4.3.1 and highlighted in Table 4.3.1.

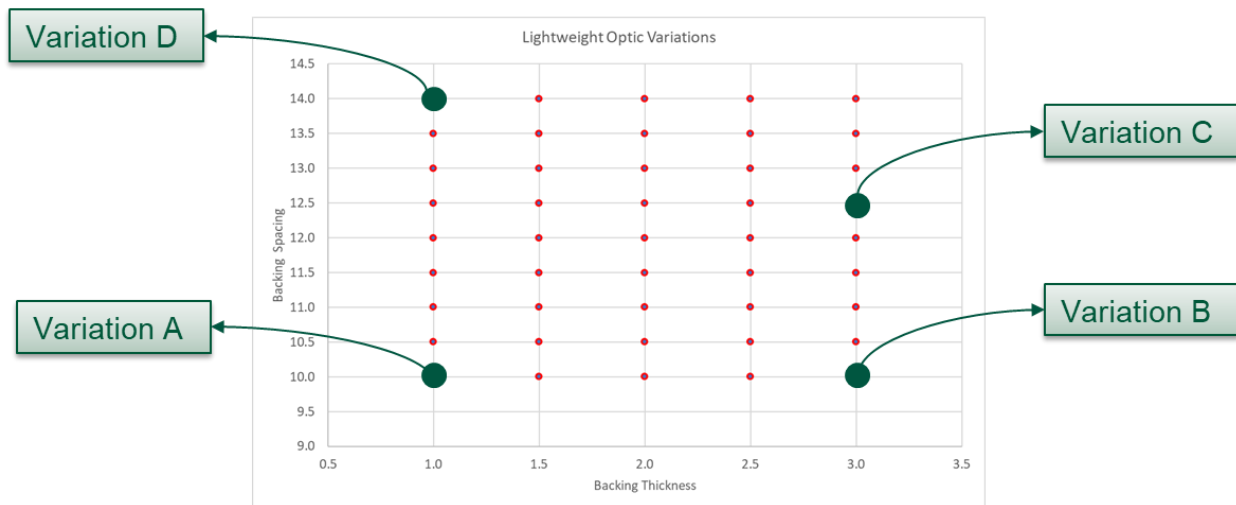


Figure 4.3.1 Lightweight Optic Variation Chart

The four different variation parameters were chosen because of the many different applications in that lightweight optics can be used that might require different specifications. These four variations tested the longevity of the optic by performing the single pulse simulation six times resulting in six pulses of energy over 60 a second time period for the optic with and without embedded PCM. This shows how the optic will perform over multiple engagements of the directed energy weapon.

Although four optic variations are being tested the performance comparison is only comparable between the no PCM and PCM simulations of each optic. Each variation chosen was compared for the temperature after every pulse of energy as well as the displacement after each pulse.

Variation A

Variation A also known as Isogrid 10-1 can be seen in Figure 4.3.2 was chosen for being the overall best optic.

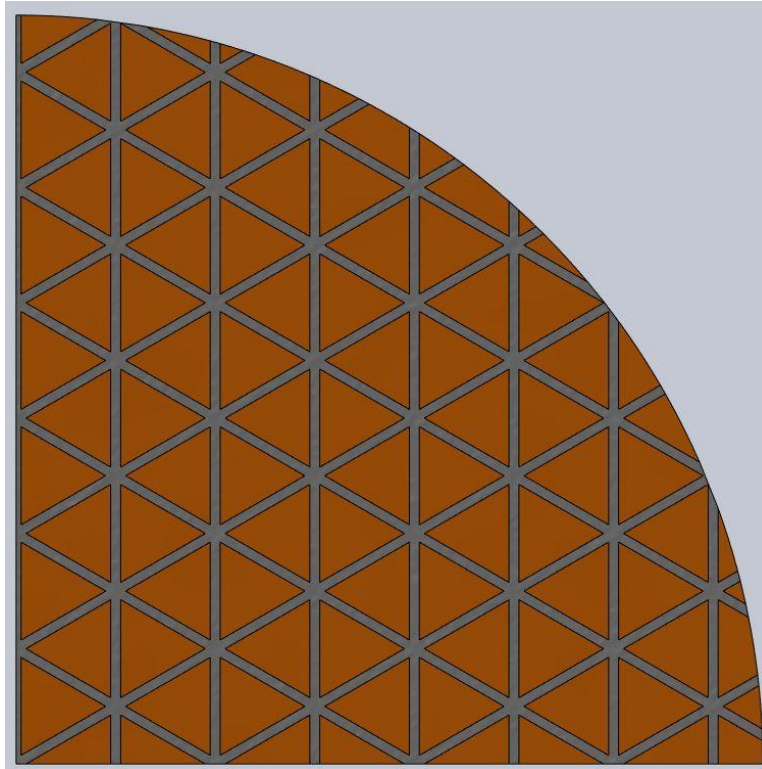


Figure 4.3.2 Variation A Backing with PCM

Additionally, Figure 4.3.3 shows the transient thermal simulation results at the 31-second mark for both with and without PCM. The results show pockets of warmer material throughout the mirror on the left without PCM. Also, it can be seen that the temperature in the mirror on the right with PCM is evenly distributed through the mirror.

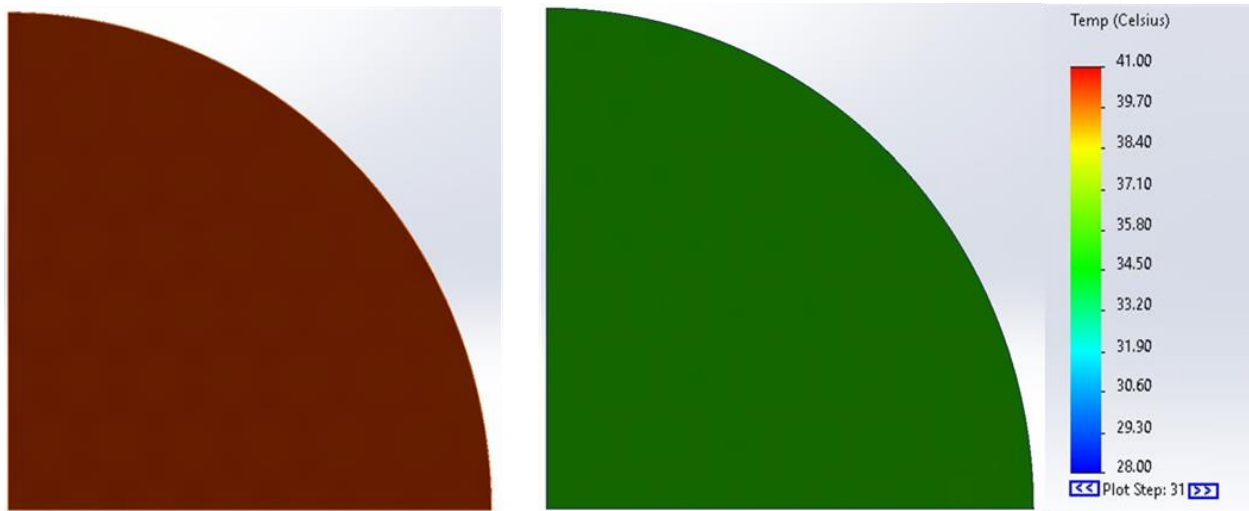


Figure 4.3.3 Variation A (Left) Without PCM (Right) With PCM

The multiple pulse simulation results showed that after the last pulse of energy, the temperature was reduced by 10.5 degrees Celsius, and the deformation was reduced by 54.9% when the PCM was present. Figures 4.3.4 and 4.3.5 show the temperature comparison and deformation comparison respectively.

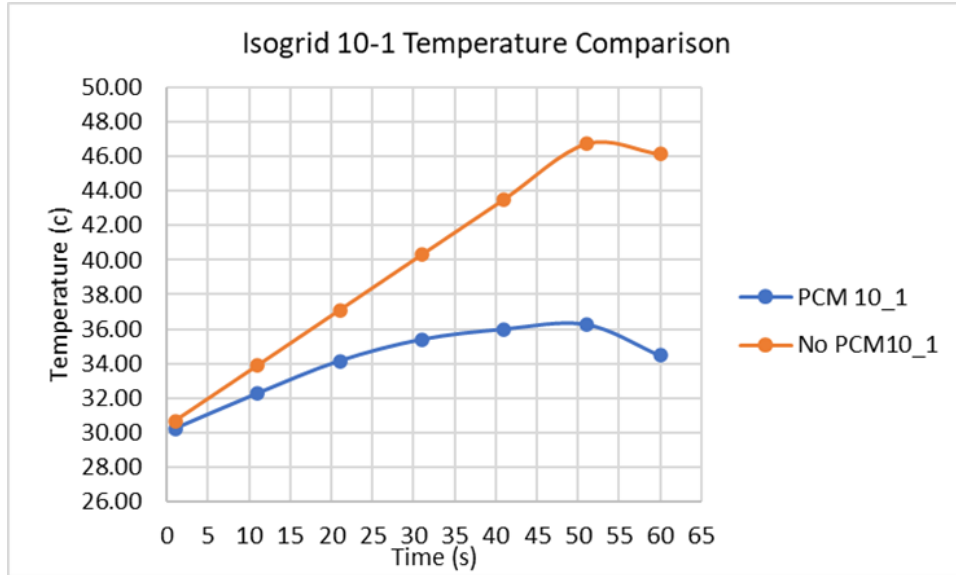


Figure 4.3.4 Variation A Maximum Temperature Comparison

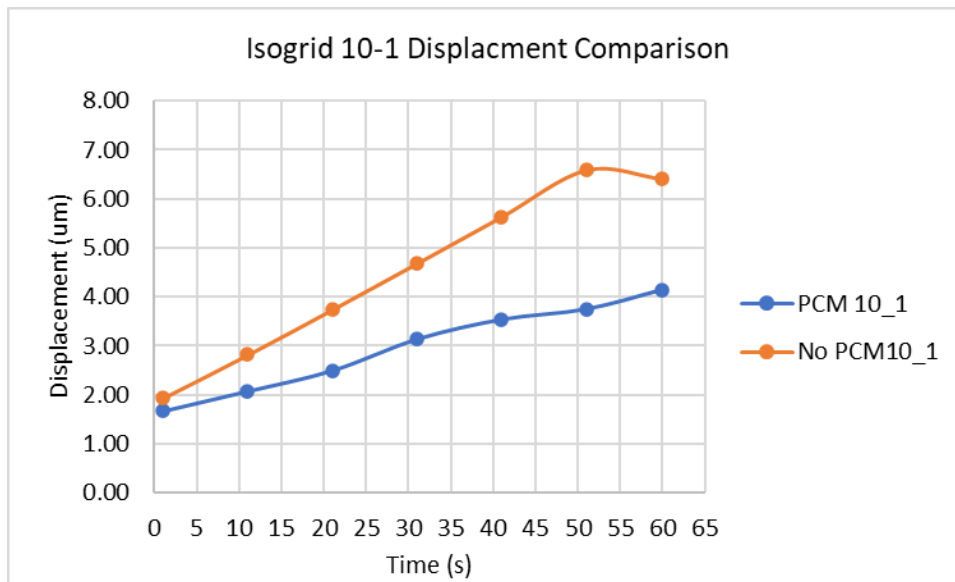


Figure 4.3.5 Variation A Maximum Deformation Comparison

Variation B

Variation B also known as Isogrid 10-3 seen in Figure 4.3.6 was chosen because it had the smallest displacement of all variations tested with PCM.

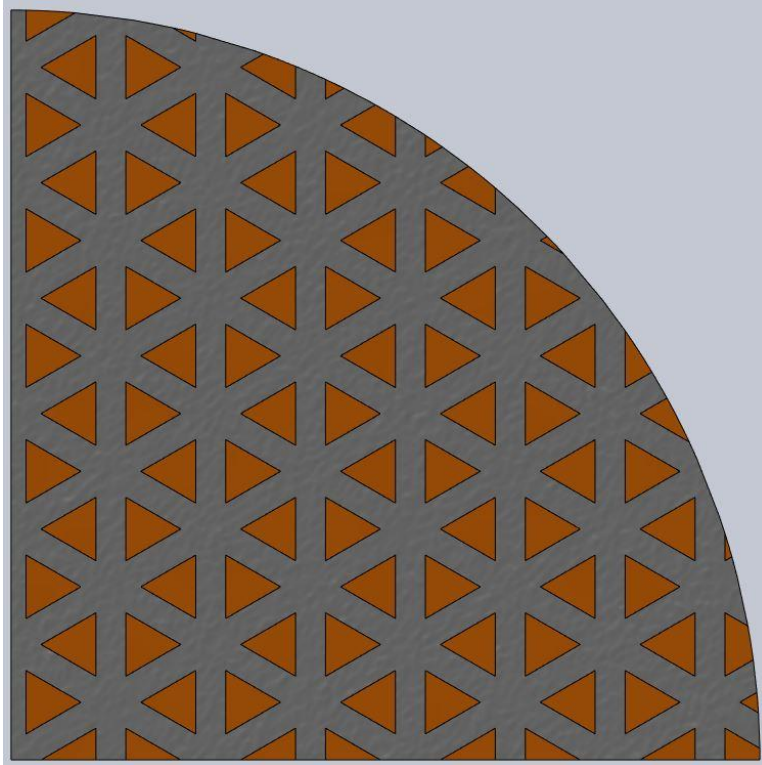


Figure 4.3.6 Variation B Backing with PCM

Figure 4.3.7 Similar to Variation A shows the pockets of warmer areas of material in the transient simulations without PCM on the left and an evenly distributed temperature throughout the optic on the right with PCM included.

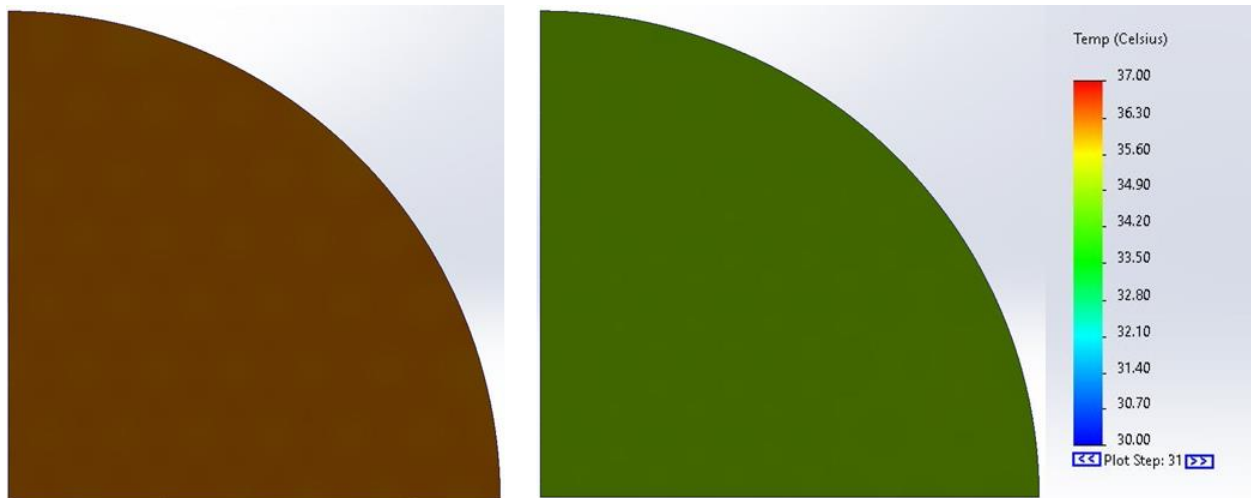


Figure 4.3.7 Variation B (Left) Without PCM (Right) With PCM

The multiple pulse simulation results showed that after the last pulse of energy, the temperature was reduced by 4.21 degrees Celsius, and the deformation was reduced by 49.9% when the PCM was present. Figures 4.3.8 and 4.3.9 show the temperature comparison and deformation comparison respectively.

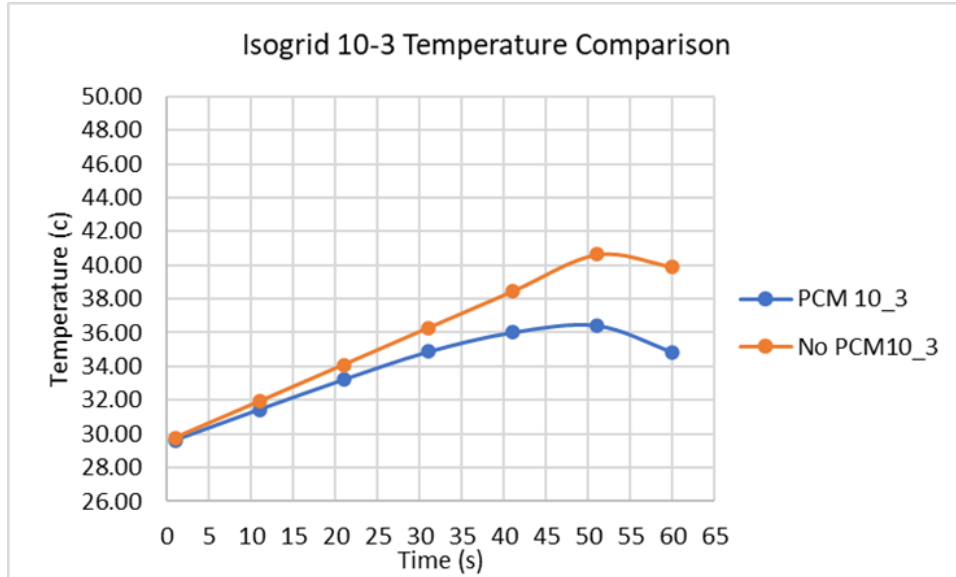


Figure 4.3.8 Variation B Maximum Temperature Comparison

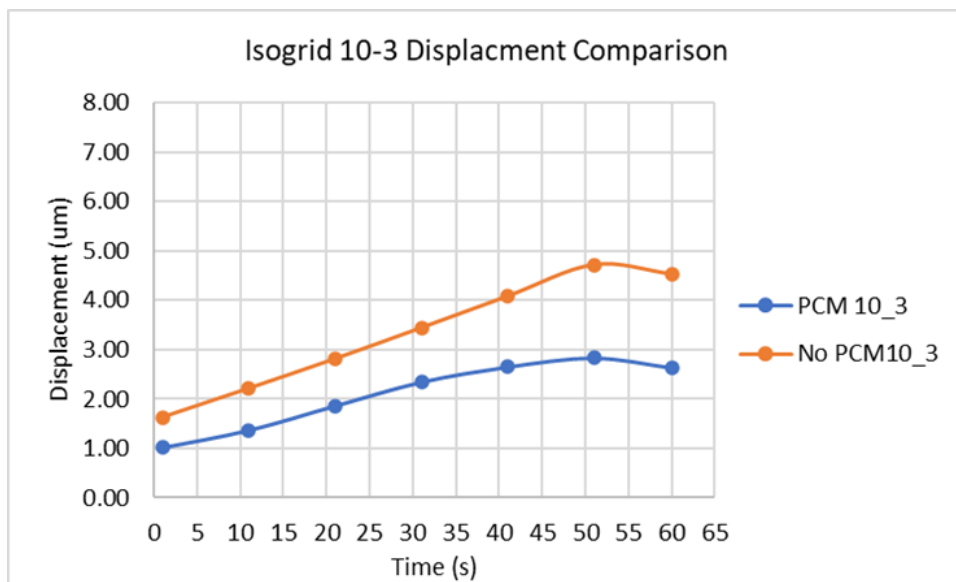


Figure 4.3.9 Variation B Maximum Deformation Comparison

Variation C

Variation C also known as Isogrid 12.5-3 seen in Figure 4.3.10 was chosen because it had the lowest temperature after the singular pulse of energy.

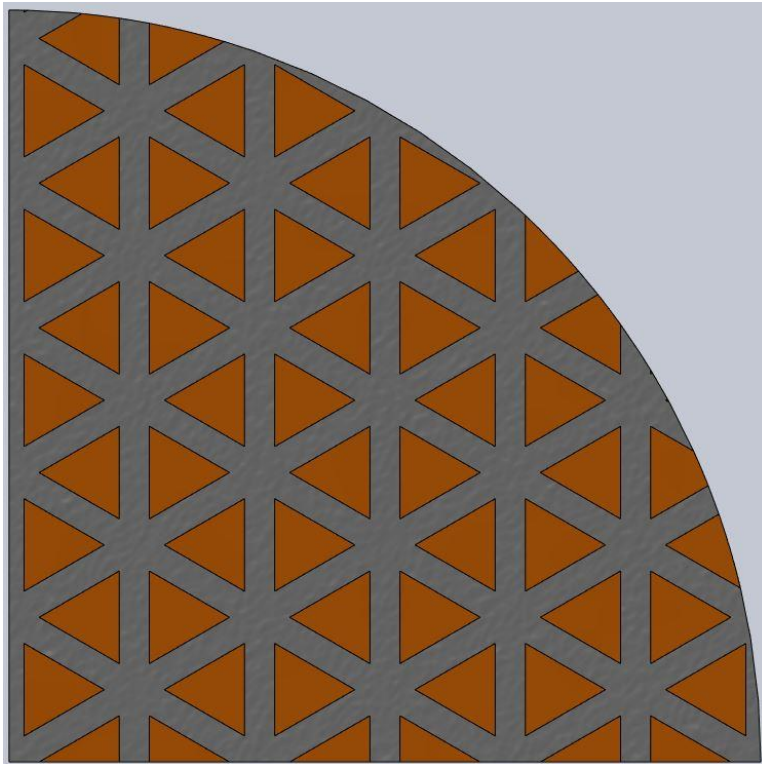


Figure 4.3.10 Variation C Backing with PCM

Figure 4.3.11 shows the simulations Variation C at the 31 second point within the transient thermal simulations. One key difference then the variations previously mentioned is that the simulation without PCM has larger pockets of increased temperature variance across the mirror face.

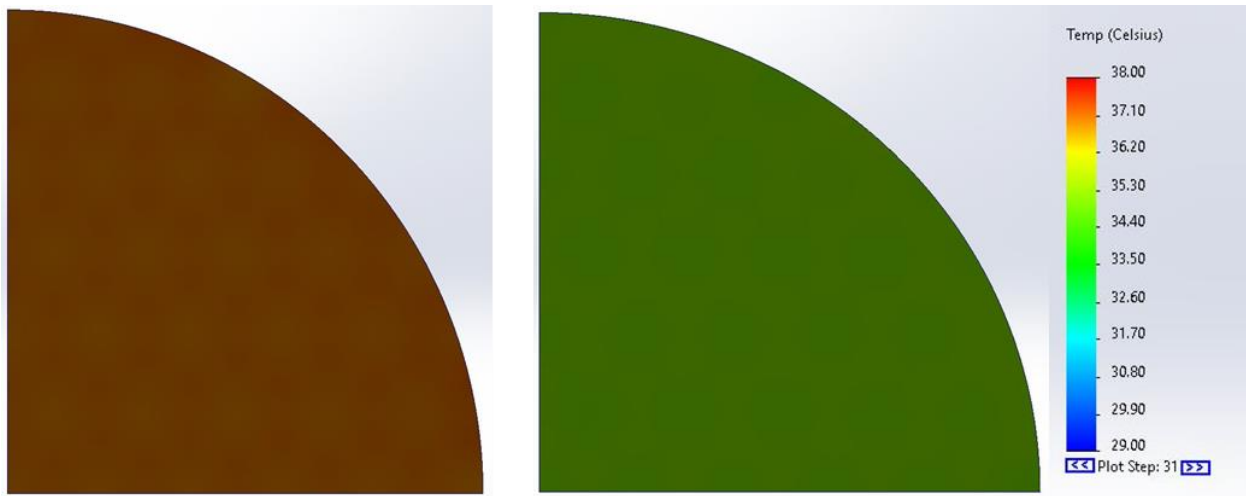


Figure 4.3.11 Variation C (Left) Without PCM (Right) With PCM

The multiple pulse simulation results showed that after the last pulse of energy, the temperature was reduced by 5.39 degrees Celsius, and the deformation was reduced by 46.6% when the PCM was present. Figures 4.3.12 and 4.3.13 show the temperature comparison and deformation comparison respectively.

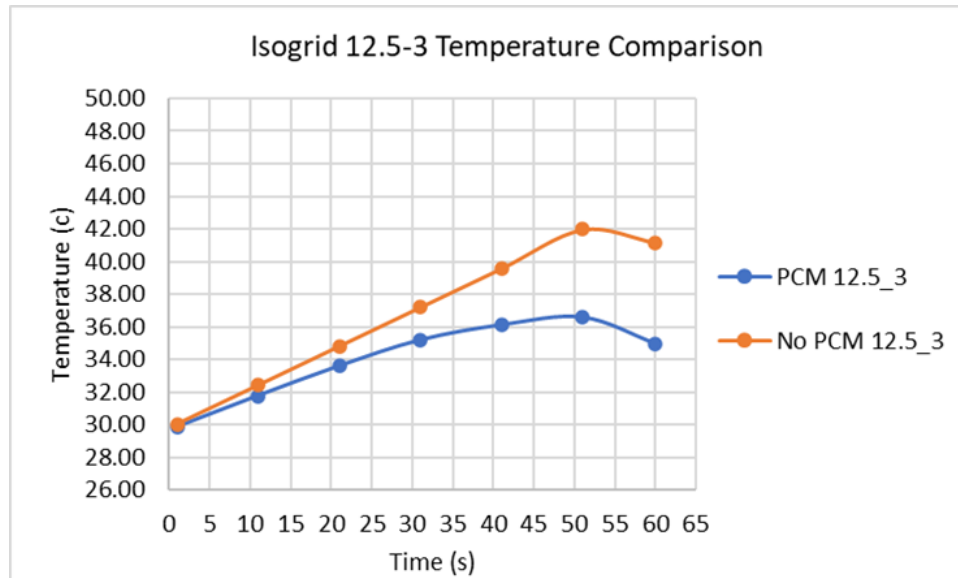


Figure 4.3.12 Variation C Maximum Temperature Comparison

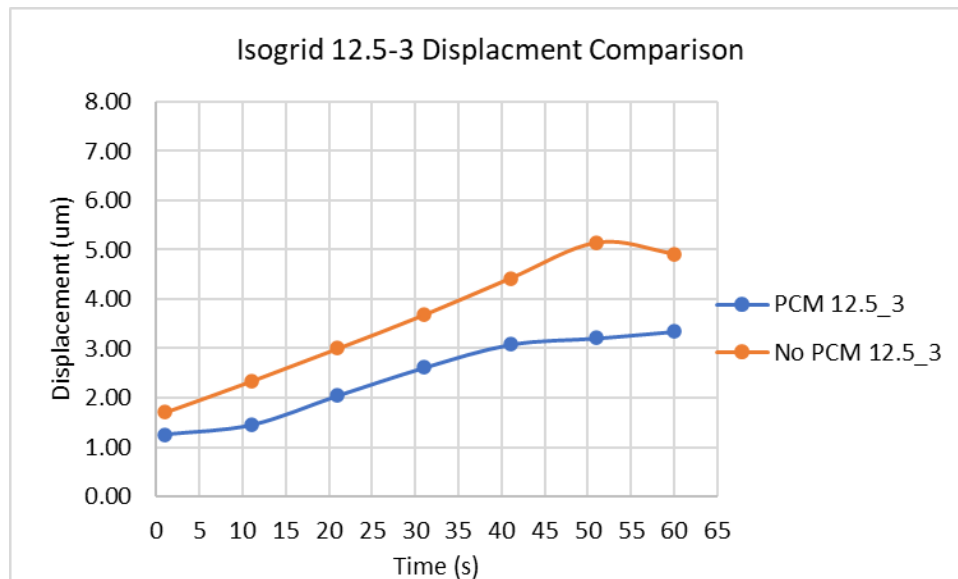


Figure 4.3.13 Variation C Maximum Deformation Comparison

Variation D

Variation D also known as Isogrid 14-1 seen in Figure 4.3.14 was chosen because it had the lowest areal density of all variations.

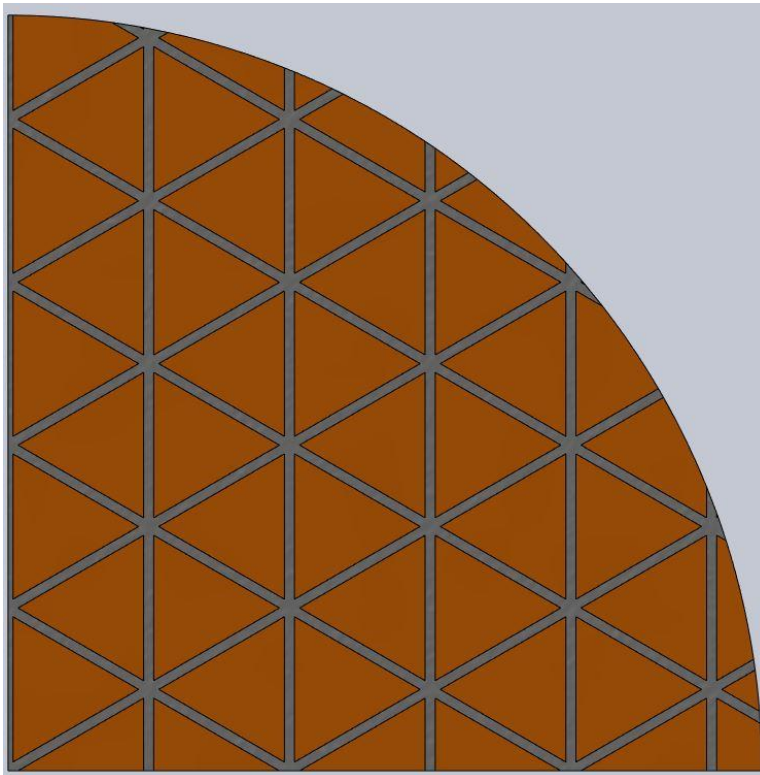


Figure 4.3.14 Variation D Backing with PCM

Figure 4.3.15 showcases the simulations Variation C at the 31-second point within the transient thermal simulations. This variation shows a wide temperature variation from no PCM to PCM simulations where the non-PCM variation shows similar pockets as the other variations but the PCM variation shows an even distribution on this temperature scale.

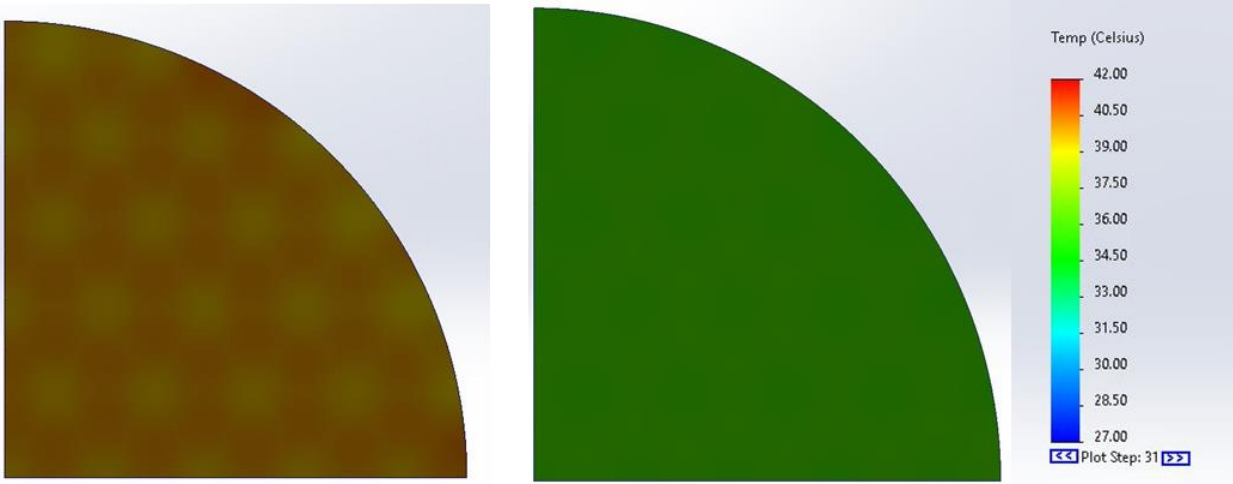


Figure 4.3.15 Variation D (Left) Without PCM (Right) With PCM

The multiple pulse simulation results showed that after the last pulse of energy, the temperature was reduced by 11.64 degrees Celsius, and the deformation was reduced by 18.3% when the PCM was present. Figures 4.3.16 and 4.3.17 show the temperature comparison and deformation comparison respectively.

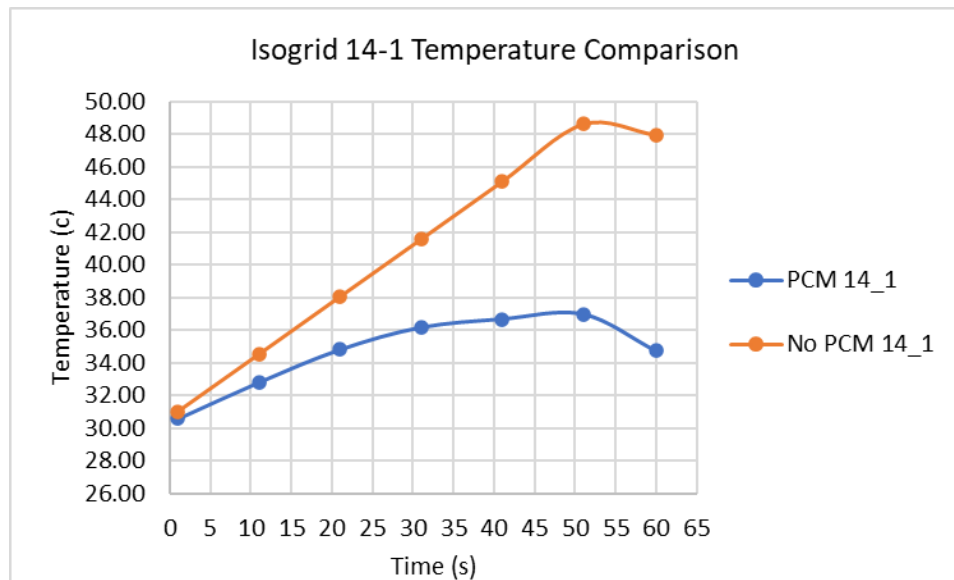


Figure 4.3.16 Variation D Maximum Temperature Comparison

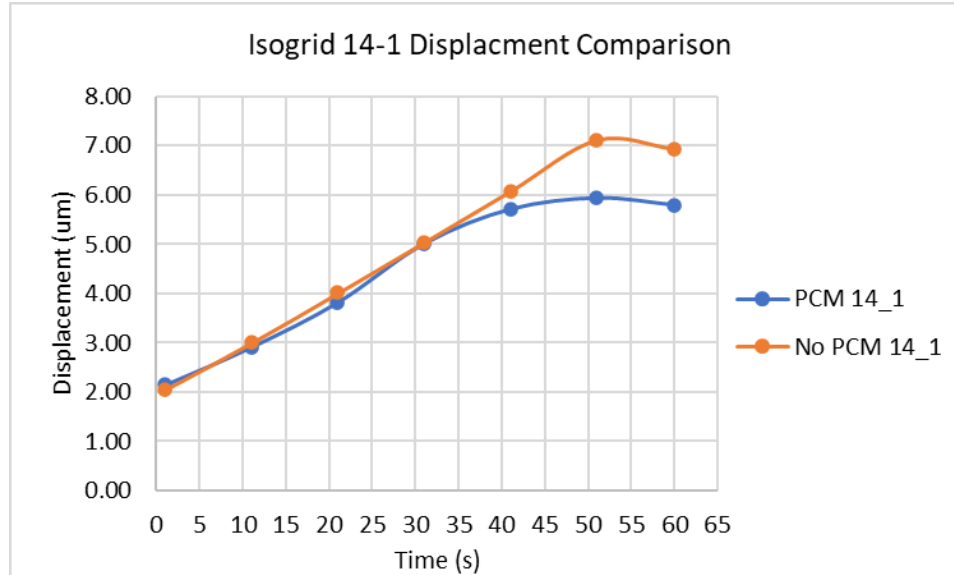


Figure 4.3.17 Variation D Maximum Deformation Comparison

Each Isogrid variation had a lower temperature with PCM embedded into the backing of the optics. As a result, the deformation after the last pulse of energy was also lower in every variation.

The simulations to this point all were performed using pulses of energy that allow the energy to absorb into the optic when the energy was not applied. To show all performance aspects of the PCM-embedded optic a final simulation was performed that was a constant energy that would result in the same amount of energy as the pulsed simulations. Due to the overall versatility of Variation A, it was chosen as the optic to be investigated for this last simulation. The energy that both optics saw for their simulations was 180 kJ total in which only 3.6 kJ was absorbed, resulting in 600 J for the full optic and 150 J for the quarter model. Figures 4.3.18 and 4.3.19 show the temperature comparison and deformation comparison respectively.

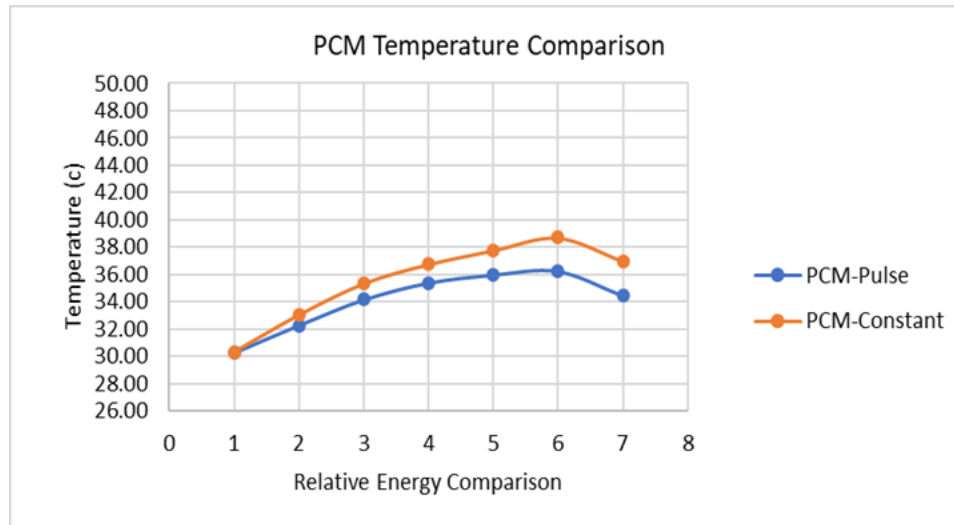


Figure 4.3.18 Variation A Energy Delivery Maximum Temperature Comparison

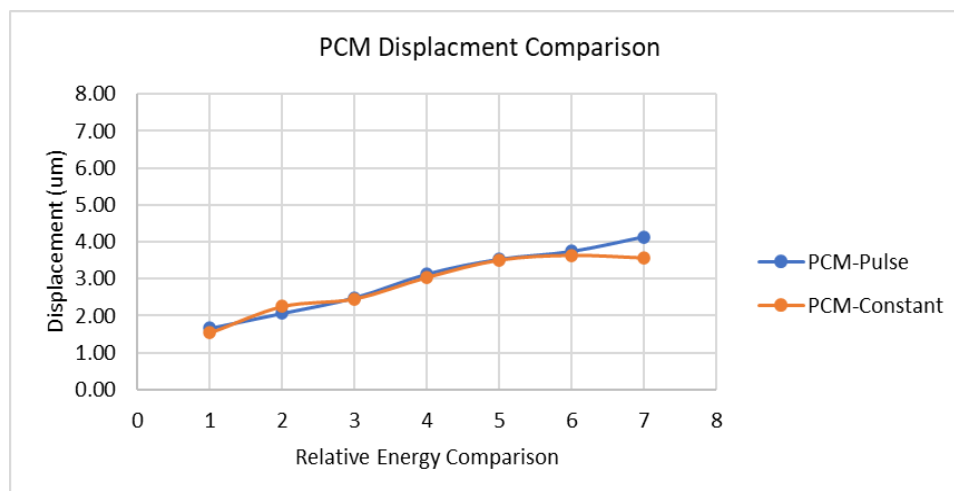


Figure 4.3.19 Variation A Energy Delivery Maximum Deformation Comparison

As expected, the constant energy optic held a hotter temperature due to its inability to distribute the thermal energy throughout the optic and PCM as well as the pulsed energy simulation. Even with the increased temperature the constant energy optic holds a similar deformation pattern as the pulsed energy optic simulation. Although the temperature was increased in the constant energy simulation it can be seen that the PCM was able to absorb a large amount of the energy holding the temperature below the temperature without PCM.

4.4 Highlights of Results

Lumped Capacitance Simulations

- Successfully demonstrated the addition of PCM reduced the maximum temperature by 58.6%.
- Conduction within the mirror layers is high causing the layers to increase in temperature similarly.
- 1D Simscape simulation with PCM included following the characteristics of phase change seen in Figure 2.3.1

Thermal Finite Element Analysis

- A relationship between the areal density and maximum temperature can be made when the areal density increases the maximum temperature is decreased and inversely as the areal density is decreased the maximum temperature is increased.
- After the 45 different Isogrid variation simulations the variation with the lowest temperature was Isogrid 10-3 with a maximum temperature of 29.8 degrees Celsius.

Thermal-Mechanical Finite Element Analysis

- The average temperature across the four final variations with PCM included was decreased by 19.3% or 7.9 degrees Celsius.
- The average deformation across the four final variations with PCM included was decreased by 42.3% or 2.0 micrometers.
- On average the increase in areal density was an additional $2.3 \frac{mg}{mm^2}$

Chapter 5 Conclusion & Discussion

5.1 Lumped Capacitance Simulations

The lumped capacitance simulation method was chosen initially for the low computational resources needed to complete a high-level investigation into if adding a mass of PCM to a mass of optic material would aid in the reduction of the maximum temperature. Whereas if the temperature was reduced within the optic as a result of the added PCM, it could reduce the distortion across the mirror face, increasing the overall effectiveness of the mirror. This model includes multiple layers within each material for increased visibility into how the heat is conducting throughout the two materials. This performance insight allows the designer to manipulate each material by adding and subtracting layers to show the response such that if the lower layers of the phase change material are not conducting the thermal energy efficiently then the material can be removed to see if the desired results are still being achieved.

With the phase change of the paraffin set at 35 degrees Celsius, the PCM effectively reduced the maximum temperature by 58.6% which is equivalent to 53.7 degrees Celsius. Additionally, the response is shown in Figure 4.1.3. held the same characteristics as the heating section of the temperature curve in Figure 2.3.1. Where Section 1 was the sensible heating of the PCM with each pulse of the laser, Section 2 absorbed energy to allow for the PCM to melt, and lastly Section 3 where the PCM has fully melted, and the sensible heating of the optic material continues. As previously mentioned, if convective cooling was included in the simulations the response would resemble that of the cooling cycle within Figure 2.3.1.

5.2 Thermal Finite Element Analysis

The thermal finite element analysis simulations were developed following the successful 1D lumped capacitance simulations. Understanding that the 1D simulations did not take the geometric backing into account it was inferred, to begin with, that the thermal finite element analysis simulations would perform similarly but would increase the overall fidelity of the mirror's response to the PCM. The parametric optimization of the Isogrid backing initially highlighted a relationship between the areal density of a specific optic and the maximum temperature at which the optic had been seen after one pulse of energy. Namely, the lower the areal density the higher the maximum temperature would be, and inversely the higher the areal density would result in a lower maximum temperature. One of this phenomenon's driving factors was the rib spacing within the mirror backing. If the spacing was smaller, then the surface area (and available thermal mass) would be increased resulting in lower temperatures and inversely if the spacing was larger there would be less surface area (and lower thermal mass) to help reduce the temperature. This was highlighted when PCM was introduced because the higher the surface area allowed for the phase change material to absorb energy more efficiently ultimately keeping the optic at an evenly distributed temperature. This can be seen directly when comparing Isogrid 10-1 with PCM seen in Figure 5.2.1 where the temperature gradient is the same across the mirror and Isogrid 14-1 with PCM seen in Figure 5.2.2 has spots that are uneven due to the uneven melting of PCM which is directly related to the reduced surface area interacting with the PCM. It is important to note that the scale was slightly altered to illustrate the comparison better.

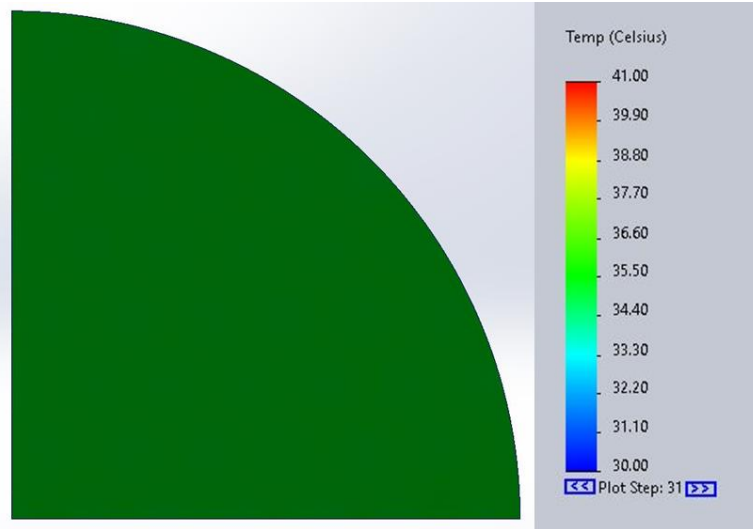


Figure 5.2.1 Isogrid 10-1 with PCM

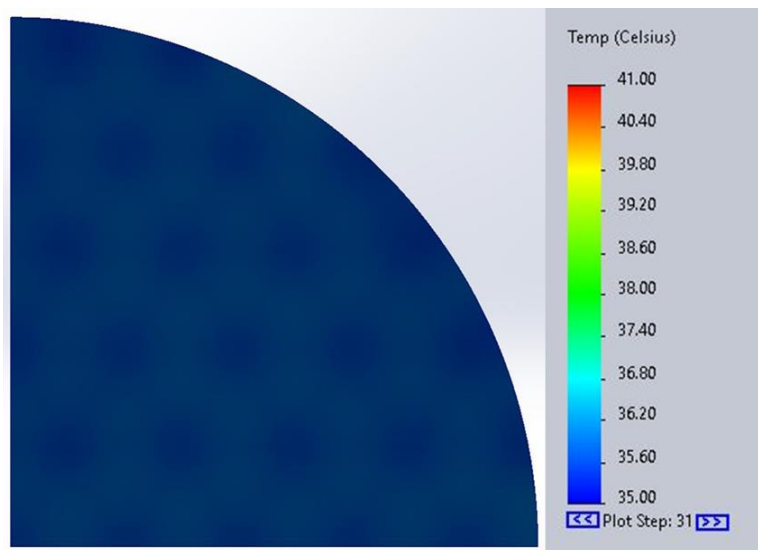


Figure 5.2.2 Isogrid 14-1 with PCM

Following the controlled simulations with no PCM nine variations were chosen to include PCM. Similar results would be expected if different variations were chosen where the PCM variations were superior to the non-PCM variations in respect of thermal management.

5.3 Thermal-Mechanical Finite Element Analysis

The second variation of the thermal simulations was focused on understanding how the thermal loading of the mirror with and without PCM would change the deformation across the mirror face. The nine variations chosen in the initial thermal simulations were all embedded with paraffin wax and run through a single energy pulsed simulation. Figure 5.3.1 is a graph of the displacement against the areal density. This shows how even with the increased areal density due to the PCM being included that in most cases the variations that do include the PCM result in a lower displacement after a single pulse of energy.

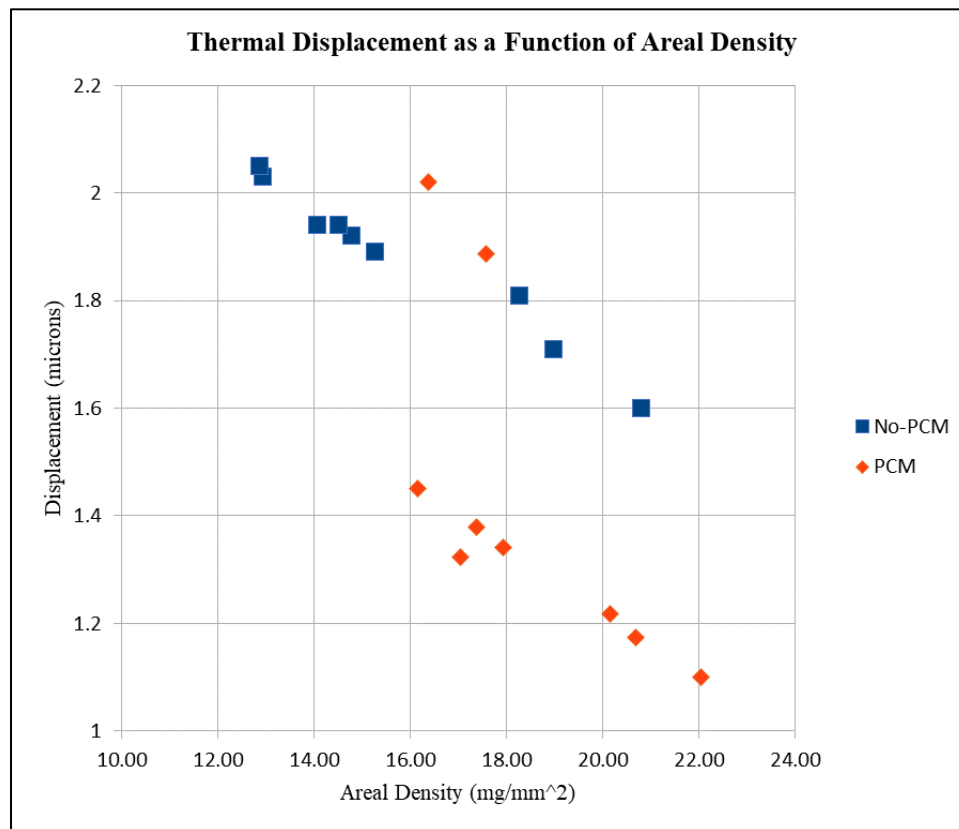


Figure 5.3.1 Thermal Displacement as a Function of Areal Density

Additionally, to narrow down the variations to only four Isogrid variations to run multiple pulse simulations a few identifying characteristics were chosen to select the variations. The

characteristics were the lowest temperature after a single pulse, lowest areal density, lowest deformation after a single pulse, and then a generalized score which was outlined in Chapter 3.2.3. Figure 5.3.2 shows a graphical representation of the results of the normalized score in comparison to the areal density. Having a low normalized score is good overall because it means that the areal density and max displacement together are low indicating it is not an optic that has characteristics with extreme ranges making it a stable optic.

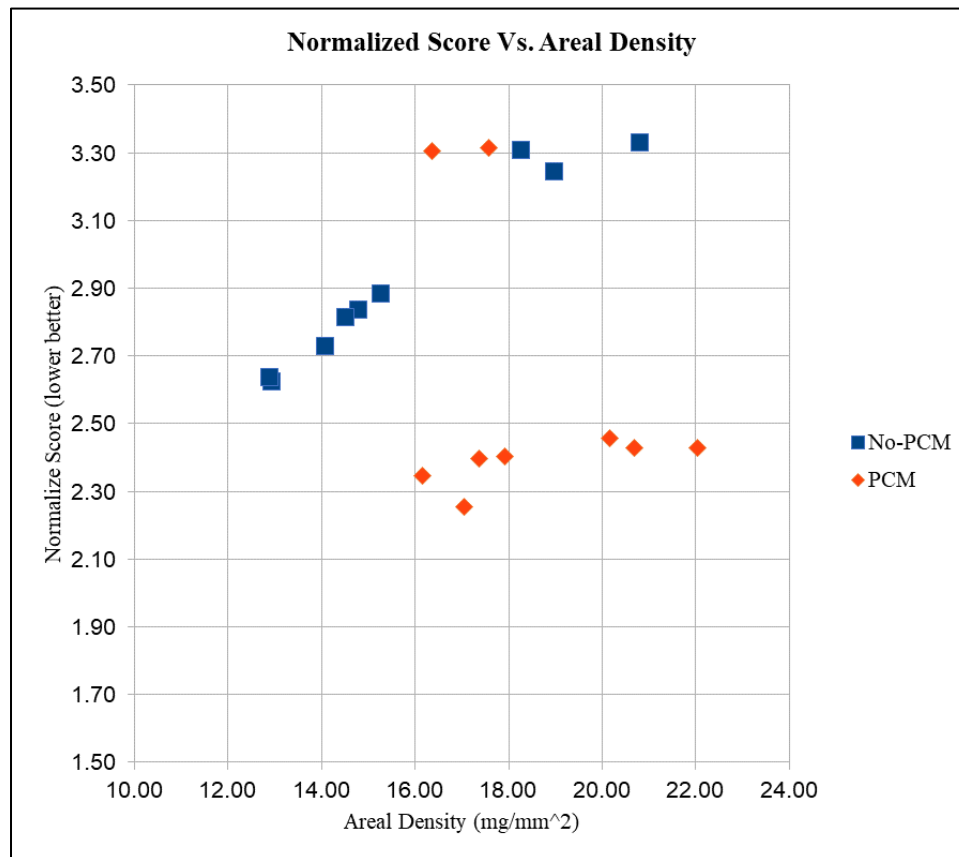


Figure 5.3.2 Normalized Score Vs. Areal Density

On average, the four Isogrid variations with the addition of PCM only added $2.3 \frac{mg}{mm^2}$ to the optics areal density. The thermal capacity increase aids in reducing the temperature with the lightweight optic and the optic's deformation, which increases the optic's dimensional stability. The average temperature across the four variations was reduced by 19.3% or 7.9 degrees Celsius.

In addition, the deformation across the four variations was reduced by 42.3% or 2.0 micrometers. Figure 5.2.3. illustrates the final comparison between the four Isogrid variations with and without PCM. This figure shows a stock chart with the max and min deformation across the face of the mirror as the tails. The box is made from a standard deviation above and below the average deformation across the mirror face. For optical design, the absolute distortion (piston) of the mirror face is less of a concern than the relative distortion of adjacent regions (waviness, ripple, etc.) which will degrade the focus of the beam.

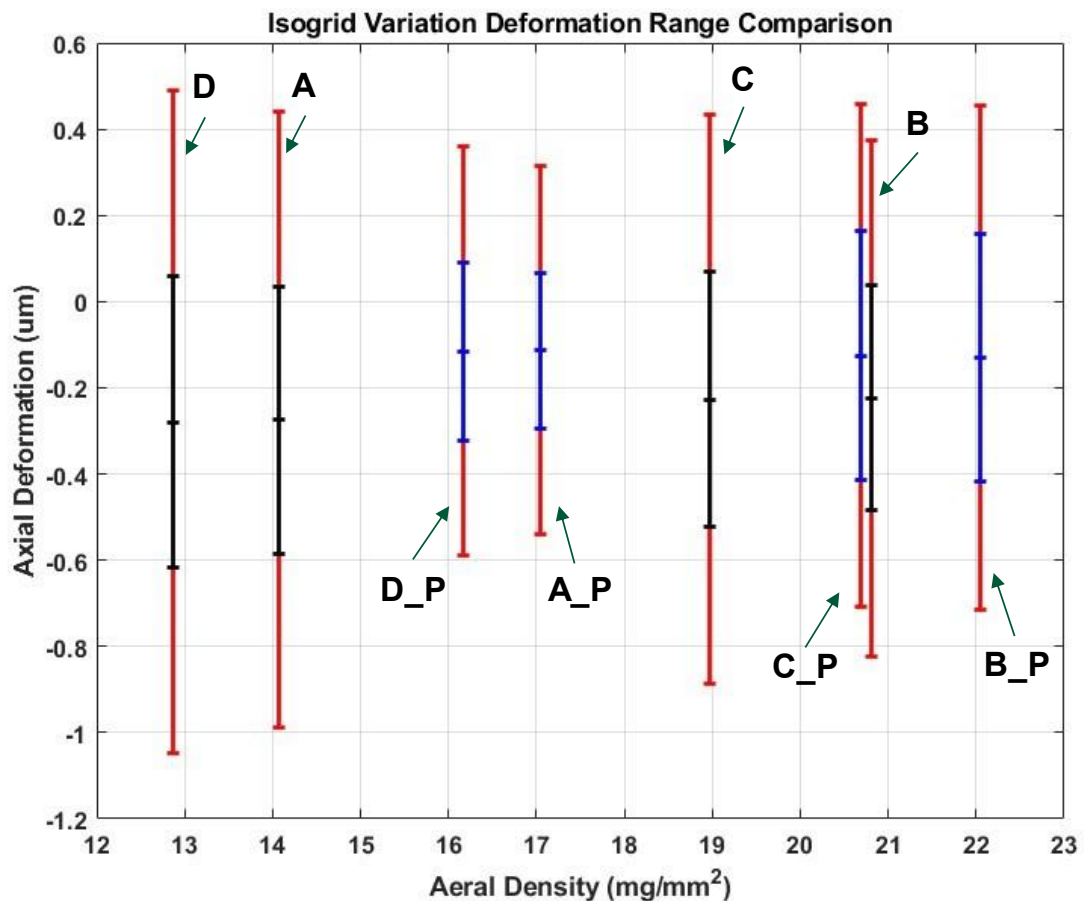


Figure 5.3.3 Isogrid Variation Deformation Range Comparison

It is important to note that variations that include an underscore P in Figure 5.3.3 are to notate the PCM. Also important is that every Isogrid variation that includes PCM has a smaller

range of deformation than the Isogrid variations without PCM. It is important to also recognize that while the Isogrid backing design parameters were swept over the previously discussed rib thickness and spacing ranges, the combinations featured in designs A and D above are most representative of an aggressively lightweight mirror design. The improvements in the thermal deformation variance for the A and D designs are also the most significant of any that were simulated, indicating an opportunity for the proposed approach.

Ultimately, alluding that embedding PCM into the backing of lightweight optics results in increased thermal capacity within the lightweight mirror allowing for increased dimensional stability which will increase the effectiveness by improving the quality of the beam on target due to the reduced distortion across the optic face.

5.4 Future Work

The potential next steps in continuing this research would include modification of lightweight optics, investigation of different exotic phase change materials, and lastly would be to perform other simulations. The lightweight optic modifications would focus on a mountable optic structure by including an enclosure to retain the PCM through the full cycle of the phase change. Also includes the addition of mounting points to the optic design which will increase the strength of the optic. Lastly, developing a physical subject to be able to physically perform the simulated test to validate computer-based simulations.

The next continuation of work would be to investigate different exotic phase change materials. This could include different materials altogether that would have better performance or an increased thermal conductivity such as vanadium dioxide. Another option could be investigating doping paraffin wax with other higher-performing phase change materials that would alter the response when heated or that would interact in a way such that when the paraffin

was done changing phase the next material would begin changing phase. This could increase the energy duration or allow for higher energy pulses of energy. The last potential phase change material alteration could be investigating the quantity of phase change within the Isogrid backing. For example, if a specific application had known operating parameters and needed to reduce the mass the PCM could be removed so that the lightweight optic performed was able to still have reduced temperature and deformation through the duration of the application.

The last focus of future work would be improving the fidelity of tests and simulations performed. This would include incorporating convective cooling into the lightweight optic simulations in both Simscape and Solidworks. Additionally, performing an in-depth optical analysis of the thermal distortion with and without PCM.

References

1. Department of Defense Joint Publication 3-13.1, Electronic Warfare (Washington, DC: Department of Defense, 2012). <https://irp.fas.org/doddir/dod/jp3-13-1.pdf>
2. Sensors and Directed Energy, Richard White, March 2021
<https://www.mda.mil/global/documents/pdf/Mr.%20Richard%20White%20Sensors%20and%20Directed%20Energy.pdf>
3. Baxi, C.B. & Knowles, Timothy. (2006). Thermal energy storage for solid-state laser weapons systems. *J. Directed Energy*. 1. 293-308.
4. Clarkson W.A. Thermal effects and their mitigation in end-pumped solid-state lasers *J. Phys. D Appl. Phys.*, 34 (2001), pp. 2381-2395
5. High-Energy Laser Weaponry Delivers Speed-of-Light ‘Hard Kills’ to Drones.
<https://www.laserfocusworld.com/lasers-sources/article/14277939/highenergy-laser-weaponry-delivers-speedoflight-hard-kills-to-drones>.
6. Pike, John. Laser Weapon System Demonstrator (LWSD),
<https://www.globalsecurity.org/military/systems/ship/systems/lwsd.htm>.
7. “Laser Trailblazer: Navy Conducts Historic Test of New Laser Weapon System.” United States Navy, <https://www.navy.mil/Press-Office/News-Stories/Article/2998829/laser-trailblazer-navy-conducts-historic-test-of-new-laser-weapon-system/>.
8. Nielsen, Philip E. *Effects of Directed Energy Weapons*. NDU Press, 1994
9. Concentrating solar-thermal power basics (no date) Energy.gov. Available at:
<https://www.energy.gov/eere/solar/concentrating-solar-thermal-power-basics> (Accessed: October 15, 2022).

10. Power Tower System concentrating solar-thermal power basics Energy.gov. Available at: <https://www.energy.gov/eere/solar/power-tower-system-concentrating-solar-thermal-power-basics> (Accessed: October 15, 2022).
11. Guang Liu, Liang Guo, Xintong Wang, Qingwen Wu, "Topology and parametric optimization based lightweight design of a space reflective mirror," *Opt. Eng.* 57(7) 075101 (5 July 2018)
12. "Light Weight Mirrors for Satellite & Astronomical Telescopes." *Optical Surfaces Limited*, 17 Sept. 2015, <https://www.optisurf.com/index.php/light-weight-mirrors-for-satellite-astronomical-telescopes/#:~:text=Optical%20Surfaces%20light%20weight%20mirrors,overall%20cost%20of%20the%20telescope.>
13. Nicholas Horvath and Matthew Davies, "Advancing lightweight mirror design: a paradigm shift in mirror preforms by utilizing design for additive manufacturing," *Appl. Opt.* 60, 681-696 (2021)
14. Michael Sweeney, Martyn Acreman, Tom Vettese, Ray Myatt, Mike Thompson, "Application and testing of additive manufacturing for mirrors and precision structures," *Proc. SPIE 9574, Material Technologies and Applications to Optics, Structures, Components, and Sub-Systems II*, 957406 (2 September 2015); <https://doi.org/10.1117/12.2189202>
15. James A. Monroe, Matthew East, Tony Hull, "ALLVAR alloy athermalization: a novel and cost-effective alternative for small to moderate sized space telescopes," *Proc. SPIE 11820, Astronomical Optics: Design, Manufacture, and Test of Space and Ground Systems III*, 118200B (24 August 2021); <https://doi.org/10.1117/12.2594816>

16. He, Rujie, Niping Zhou, Keqiang Zhang, Xueqin Zhang, Lu Zhang, Wenqing Wang, and Daining Fang. "Progress and challenges towards additive manufacturing of SiC ceramic." *Journal of Advanced Ceramics* 10, no. 4 (2021): 637-674.
17. Ronald Plummer, Don Bray, "Guidelines for design of SuperSiC silicon carbide mirror substrates and precision components," *Proc. SPIE 4771, Optomechanical Design and Engineering 2002*, (9 September 2002); <https://doi.org/10.1117/12.482168>
18. Righetti, Giulia, et al. "Experimental Investigation of Phase Change of Medium/High Temperature Paraffin Wax Embedded in 3D Periodic Structure." *International Journal of Thermofluids*, vol. 5-6, 2020, p. 100035., <https://doi.org/10.1016/j.ijft.2020.100035>.
19. Korawan, Agus Dwi, et al. "3D Numerical and Experimental Study on Paraffin Wax Melting in Thermal Storage for the Nozzle-and-Shell, Tube-and-Shell, and Reducer-and-Shell Models." *Modelling and Simulation in Engineering*, vol. 2017, 2017, pp. 1–9.,
20. A Phase Change Materials Comparison Vegetable-based vs Paraffin-based PCMs. Available at: <https://www.chemicalonline.com/doc/a-phase-change-materials-comparison-vegetable-based-vs-paraffin-based-pcms-0001> (Accessed: November 22, 2022).
21. PHASE CHANGE MATERIAL (PCM) SELECTION (no date) Advance Cooling Technologies. Available at: <https://www.1-act.com/products/pcm-heat-sinks/pcmselection/> (Accessed: November 22, 2022).
22. Wang, Xiang-Qi, et al. "A Parametric Study of Phase Change Material (PCM)-Based Heat Sinks." *International Journal of Thermal Sciences*, vol. 47, no. 8, 2008, pp. 1055–1068., <https://doi.org/10.1016/j.ijthermalsci.2007.07.016>.

23. Liu, Ming, et al. "Review and Characterisation of High-Temperature Phase Change Material Candidates between 500 c and 700°C." *Renewable and Sustainable Energy Reviews*, vol. 150, 2021, p. 111528., <https://doi.org/10.1016/j.rser.2021.111528>.
24. Abdulrahman, Ruslan Sabah, et al. "Development of Paraffin Wax as Phase Change Material Based Latent Heat Storage in Heat Exchanger." *Applied Thermal Engineering*, vol. 150, 2019, pp. 193–199., <https://doi.org/10.1016/j.applthermaleng.2018.12.149>

Appendices

Appendix 1: 45 Isogrid Variations

	mm		grams		mm ²	g/mm ²	C
	Spacing	Thickness	Quarter Mass	Full Mass	Area	Areal Density	Max Temp
1	10.0	1.0	62.2	248.6	17671.5	14.1	30.7
2	10.0	1.5	70.8	283.3	17671.5	16.0	30.3
3	10.0	2.0	78.7	314.7	17671.5	17.8	30.1
4	10.0	2.5	85.7	342.8	17671.5	19.4	29.9
5	10.0	3.0	91.9	367.7	17671.5	20.8	29.8
6	10.5	1.0	61.3	245.1	17671.5	13.9	30.8
7	10.5	1.5	69.6	278.4	17671.5	15.8	30.4
8	10.5	2.0	77.2	308.6	17671.5	17.5	30.2
9	10.5	2.5	84.0	335.8	17671.5	19.0	30.0
10	10.5	3.0	90.1	360.2	17671.5	20.4	29.8
11	11.0	1.0	60.3	241.0	17671.5	13.6	30.8
12	11.0	1.5	68.2	273.0	17671.5	15.4	30.5
13	11.0	2.0	75.6	302.3	17671.5	17.1	30.3
14	11.0	2.5	82.3	329.1	17671.5	18.6	30.1
15	11.0	3.0	88.3	353.2	17671.5	20.0	29.9
16	11.5	1.0	59.7	238.8	17671.5	13.5	30.9
17	11.5	1.5	67.4	269.6	17671.5	15.3	30.6
18	11.5	2.0	74.5	298.0	17671.5	16.9	30.3
19	11.5	2.5	81.0	324.0	17671.5	18.3	30.1
20	11.5	3.0	86.9	347.6	17671.5	19.7	30.0
21	12.0	1.0	59.1	236.5	17671.5	13.4	30.8
22	12.0	1.5	66.6	266.6	17671.5	15.1	30.5
23	12.0	2.0	73.6	294.3	17671.5	16.7	30.3
24	12.0	2.5	80.0	319.9	17671.5	18.1	30.1
25	12.0	3.0	85.8	343.2	17671.5	19.4	29.9
26	12.5	1.0	57.1	228.4	17671.5	12.9	31.0
27	12.5	1.5	65.3	261.1	17671.5	14.8	30.6
28	12.5	2.0	72.0	287.8	17671.5	16.3	30.4
29	12.5	2.5	78.1	312.6	17671.5	17.7	30.2
30	12.5	3.0	83.8	335.3	17671.5	19.0	30.0
31	13.0	1.0	57.7	230.8	17671.5	13.1	31.0
32	13.0	1.5	64.6	258.6	17671.5	14.6	30.7
33	13.0	2.0	71.1	284.5	17671.5	16.1	30.4
34	13.0	2.5	77.2	308.7	17671.5	17.5	30.3
35	13.0	3.0	82.4	329.6	17671.5	18.7	30.1
36	13.5	1.0	57.3	229.3	17671.5	13.0	31.0
37	13.5	1.5	64.1	256.5	17671.5	14.5	30.7
38	13.5	2.0	70.5	281.9	17671.5	16.0	30.4
39	13.5	2.5	76.4	305.5	17671.5	17.3	30.2
40	13.5	3.0	81.8	327.4	17671.5	18.5	30.1
41	14.0	1.0	56.9	227.5	17671.5	12.9	31.0
42	14.0	1.5	63.5	253.8	17671.5	14.4	30.8
43	14.0	2.0	69.6	278.5	17671.5	15.8	30.6
44	14.0	2.5	75.4	301.5	17671.5	17.1	30.4
45	14.0	3.0	80.7	322.9	17671.5	18.3	30.2

Appendix 2: Custom PCM Block Code

```

component PCmass
% Thermal Phase Change Mass
% This block models internal energy storage in a thermal network. The rate
% of temperature increase is proportional to the heat flow rate into the
% material and inversely proportional to the mass and specific heat of the
% material.

% Copyright 2005-2017 The MathWorks, Inc.

nodes
    M = foundation.thermal.thermal; % :top
end

parameters
    mass = {1, 'kg'}; % Mass
    cpTemp={ [0 200 300 310 311 312], 'K'}; %temp values
    cp={ [2890 2890 2890 2890 200e3 2890], 'J/(kg*K)'}; % cp values
end
variables
    % Differential variables
    T = {value = {300, 'K'}, priority = priority.high}; % Temperature

    Q = {0, 'W'}; % Heat flow rate
    sp_heat={0, 'J/(kg*K)'}; % specific heat
end

branches
    Q : M.Q -> *;
end

equations
    assert(mass > 0)
    %assert(sp_heat > 0)
    sp_heat==tablelookup(cpTemp,cp,T,...
        interpolation=nearest,...
        extrapolation=nearest);
    T == M.T;
    Q == mass * sp_heat * T.der;
    assert(T > 0, 'Temperature must be greater than absolute zero')
end

end

```